JURNAL RISET
TEKNOLOGI PENCEGAHAN PENCEMARAN INDUSTRI

Research Journal of Industrial Pollution Prevention Technology

Vol. 13, No. 2, November 2022

FOCUS AND SCOPE

Jurnal Riset Teknologi Pencegahan Pencemaran Industri (Research Journal of Industrial Pollution Prevention Technology) seeks to promote and disseminate original research as well as review, related to following area:

Environmental Technology : within the area of air pollution technology, wastewater treatment technology, and management of solid waste and harzardous toxic substance.

Process Technology and Simulation : technology and/or simulation in industrial production process aims to minimize waste and environmental degradation.

Design Engineering : device engineering to improve process efficiency, measurement accuracy and to detect pollutant.

Material Fabrication : environmental friendly material fabrication as subtitution material for industry.

Energy Conservation : process engineering/ technology/ conservation of resources for energy generation.

Ir. Nilawati
National Research and Innovation Agency

Moch. Syarif Romadhon, S.Si., M.Sc.
National Research and Innovation Agency

Bekti Marlena, S.T., M.Si.
Center for Standardization and Industrial Pollution Prevention Services

Rame, S.Si., M.Si.
Center for Standardization and Industrial Pollution Prevention Services

Novarina I. Handayani, S.Si., M.Si.
Center for Standardization and Industrial Pollution Prevention Services

Rustiana Yuliasni, S.T., M.Sc.
National Research and Innovation Agency

Silvy Djayanti, S.T., M.Si.
National Research and Innovation Agency

Hanny Vistanty, S.T., M.T.
National Research and Innovation Agency

Nanik Indah Setianingsih, S.TP., M.Ling.
National Research and Innovation Agency

Evana Yuanita, S.T., M.T.
Center for Standardization and Services of Chemical, Pharmaceutical and Packaging Industries

Ella Kusumastuti, S.Si., M.Si.
Universitas Negeri Semarang

Jurnal Riset
Teknologi Pencegahan Pencemaran Industri
Volume 13 No. 2, November 2022

PREFACE

Thanks to Allahu Robbie 'Alamin, Journal of Industrial Pollution Prevention Technology (JRTPPI) again will publish scientific articles, especially in the field of environmental technology for volume 13 no 2. Our high appreciation is directed to the authors and editorial board who have actively participated so as to maintain consistency of quality and punctuality of our periodic publications. We would like to acknowledge our high appreciation to the head of Center for Standardization and Industrial Pollution Prevention Services, Ministry of Industry.

This edition of the issue is five series published that in full-text English. This continous policy is an attempt of the editorial board to improve the author's performance in delivering the results of their researches. Articles in full-text English are more likely to be read by broader audience so that it will increase the number of citations. This policy is also applied in order to actualize our hope of being a globally indexed international journal.

The articles contained in this edition consist of studies concentration of carbon dioxide in urban areas, evaluation of implementation integrated biological system industrial wastewater treatment, studies mechanical and physical properties of geopolymer concrete, kinetic analysis of chicken eggshells and membrane against synthetic dye and analysis of potential utilization geothermal combined cycle residual in industrial. The five manuscripts accepted and published in this edition are from researcher and lecturer in Indonesia. The duration of submission, review, and editing of the manuscripts ranged from 1-6 months.

Hopefully, these scientific articles may be new source of knowledge and experience for readers from academic, researcher, industry, and society at large. We realize that nothing is perfect until the improvement of all parties involved is continuously done.

Semarang, November 2022

Chief Editor

Jurnal Riset

Teknologi Pencegahan Pencemaran Industri

Volume 13 No. 2, November 2022

TABLE OF CONTENT

ABSTRACT

Haryono Setiyo Huboyo*[1], Okto Risdianto Manullang[2], Budi P Samadikun[1]

([1]Department of Environmental Engineering, Diponegoro University
[2]Department of Urban and Regional Planning, Diponegoro University)

Identifying Concentration of Carbon Dioxide at Heights of 1.5 M and 15 M in Six Locations in Urban Areas

Jurnal Riset Teknologi Pencegahan Pencemaran Industri, November 2022, Vol. 13, No. 2, p. 1-9, 8 ill, 2 tab, 21 ref

Several activities in urban areas emit CO_2 gas and the amount of the emission is closely related to land use. This will, in turn, increase global warming phenomena in urban areas. So far, the estimation of pollutant concentrations in the ambient air has been carried out at the height of human breath, and very rarely the concentration values at low-level altitudes have been studied in Indonesia. This study tries to analyze the CO_2 concentration based on different altitudes and different locations.
Measurements of this study were carried out in industrial, residential, commercial, and highway areas using drones at two altitudes of 1.5 m and 15 m. The use of altitude variations to know the homogeneity of CO_2 spatial distribution at different heights. The results of the study showed CO_2 concentrations on weekday mornings and afternoons, and weekend mornings in the sampling areas at 1.5 m and 15 m in the range of 393 – 462 ppm and 391 – 460 ppm, respectively. The statistical test showed that there is no significant CO_2 concentration difference between altitudes of 1.5 m and 15 m, with only a 0.17% difference value on average. The Tugu Industrial Estate area has the highest concentration of CO_2, while the area on Jalan Perintis Kemerdekaan has the lowest concentration.

(Author)
Keywords: Carbon Dioxide, Commercial, Housing, Industrial Estate, Unmanned Aerial Vehicles

Nanik Indah Setianingsih*[1], Agus Purwanto[2], Farida Crisnaningtyas[2], Ikha Rasti Julia Sari[2]

([1]National Research and Innovation Agency
[2]Center for Standardization and Industrial Pollution Prevention Services)

Evaluation of the Implementation Integrated Biological System Industrial Wastewater Treatment Plant: Pollutant Removal, Operational Maintenance, Estimation of Carbon Emission

Jurnal Riset Teknologi Pencegahan Pencemaran Industri, November 2022, Vol. 13, No. 2, p. 10-20, 4 ill, 9 tab, 37 ref

The development of WWTP in business activities needs to pay attention to getting appropriate WWTP that is more valuable to support sustainable development. This study aims to evaluate two systems of integrated biological WWTP; anaerobic-wetland, and anaerobic-aerobic-wetland, including the effectiveness of pollutant removal, operational and maintenance, and estimation of carbon emissions. The performance of pollutant removal was evaluated by analyzing inlet and outlet samples of WWTP. An operational and maintenance evaluation was carried out by studying the WWTP operating system and maintenance procedures supported by a literature review. Carbon emission estimation was carried out using a formula referring to the IPCC Guidelines (2006). Organic matter removal of anaerobic-aerobic-wetland WWTP in the form of BOD_5 and COD are 92.12% and 91.72%, respectively, higher than anaerobic-wetland WWTP are 88.69% of BOD_5 and 77.62% of COD. Anaerobic-aerobic-wetland WWTP needs more maintenance and operation than anaerobic-wetland WWTP. The highest carbon emission of both WWTP is 41530.91 $kgCO_2$ eq/year of anaerobic-wetland WWTP from the organic matter removal process and 46485.15 $kgCO_2$ eq/year of anaerobic-aerobic-wetland WWTP. Electrical energy consumption emits in anaerobic-aerobic-wetland WWTP is 22338 $kgCO_2$ eq/year higher than anaerobic-wetland WWTP at 4299.70 $kgCO_2$ eq/year. Total carbon emissions of anaerobic-wetland WWTP is 47404.58 $kgCO_2$ eq/year and anaerobic-aerobic-wetland WWTP is 68900.23 $kgCO_2$ eq/year.

(Author)
Keywords: Carbon emission, Integrated biological system, Pollutant removal, WWTP evaluation

Muhammad Amin*[1], Yugo Chambioso[2], Suharto[1], Roniyus Marjunus[2], Yusup Hendronursito[1]

([1]National Research and Innovation Agency
[2]Physics Department, Faculty of Mathematics and Natural Science - Universitas Lampung)

The Effect of Bentonite and Palm Shell Ash on The Mechanical and Physical Properties of Geopolymer Concrete

Geopolymer concrete is an alternative to obtaining environmentally friendly mortar by synthesizing materials that contain a lot of aluminum silicate. This study aims to determine the effect of bentonite and palm shell ash composition on geopolymers' physical and mechanical characteristics. All materials are mashed, mixed, and molded with a 5x5x5 cm^3 cube. Ten specimens were prepared with bentonite - palm shell ash compositions are 40/45, 45/40, 50/35, 55/30, and 60/25 wt%. Meanwhile, the composition of NaOH, Na_2SiO_3, superplasticizer and water remained at 1.3, 7.7, 2, and 5 wt%, respectively. Then the samples were dried at room temperature for 24 hrs and heated at 60 °C or 80 °C for 12 hrs. The geopolymer concrete with the best characteristics was obtained with a composition of 40 wt% bentonites and 45 wt% palm shell ash by heating at 80 °C. This specimen has a compressive strength of 11.94 MPa with a density of 2.42 g/cm^3, porosity of 8.43%, and absorption of 3.48%. The results have a chemical composition of 55.59% SiO_2, 9.45% Al_2O_3, and 8.22 Fe_2O_3 with a dominant quartz phase. Scanning electron microscope photo shows good bonding between particles, and there are no pores formed.

(Author)
Keywords: Bentonite, Concrete, Compressive Strength, Geopolymer, Palm Shell Ash

Linda Hevira[*1], Gampito[2]

([1]University of Mohammad Natsir, Bukittinggi, Indonesia
[2]Islamic University of Mahmud Yunus, Batusangkar, Indonesia)

The Kinetic Analysis and Adsorption Isotherm of Chicken Egg Shells and Membranes Against Synthetic Dyes

Textile industry waste at this time is enough to worry the community and the environment. The presence of synthetic dyes in water is hazardous, even in small concentrations. These synthetic dyes are derivatives of aromatic compounds such as benzene, toluene, and naphthalene, which are more resistant and stable than natural dyes. The adsorption method is used because it is easier to do, has no side effects, and does not require complicated and expensive equipment. In this study, the shells and membranes of discarded chicken eggs became useful as an absorbent of indigo carmine dye with an adsorption capacity of 6.399 mg/g. The adsorption reaction kinetics were analyzed from the optimal contact time data, and the reaction isotherm was analyzed from the adsorption optimal concentration data. The kinetic model that fits the research is the second pseudo-order with R^2 = 0.9998. The adsorption mechanism demonstrates that the adsorption capacity is proportional to the adsorbent's active sites. The adsorption isotherm model, with R^2 = 0.9748, is more closely related to the Freundlich isotherm model, indicating that adsorption occurs in several layers. From an economic point of view, chicken egg shells and membranes can be recommended as dye absorbers that are eco-friendly, efficient, and simple to obtain while lowering organic solid waste.

(Author)
Keywords: Adsorption, Dyes, Indigo Carmine, Isotherm, Reaction Kinetics

Jonius Christian Harefa[*1], Hadiyanto[2], Udi Harmoko[3]

([1]Master of Energy, Diponegoro University, Semarang, Indonesia
[2]Chemical Engineering, Diponegoro University, Semarang, Indonesia
[3]Department of of Physics, Diponegoro University, Semarang, Indonesia)

Analysis of Potential Utilization of Sarulla Geothermal Combined Cycle Residual Fluids for Direct Use in The Coffee Industry

The Geothermal Power Plant is one of the new renewable energy power plants. In Indonesia, the realization has reached 2%. Sarulla Operations Limited is the first geothermal power plant in Indonesia, located in North Tapanuli Regency, that utilizes combined cycle technology. Coffee is the leading commodity in the North Tapanuli district, with a plant area of 17,586 hectares. Coffee is dried in the traditional way (open field drying) so that it is still constrained by rain and cloudiness and can only be done during the day. The reinjection well fluid has a temperature of 103˚C with a flow rate of 4978 t/h and a pressure of 6–14 Bar. This study analyses the residual fluid energy for coffee drying purposes. Energy and exergy calculations are done manually and using DWSIM software with a total of 24 data points 24 hours a day to represent the availability of dryers both day and night. The results showed that the most energy needed to raise the drying air temperature at night from 15°C to 60°C was 125.62 kW, while the lowest energy needed to raise the drying air temperature during the day from 30°C to 40°C was 27.92 kW. The results of research calculations show the energy potential for residual fluid from geothermal plants to be used for drying coffee for 24 hours, both day and night.

(Author)
Keywords: Coffee, Direct Use, Geothermal, Residual Fluids, Sarulla

Identifying Concentration of Carbon Dioxide at Heights of 1.5 M and 15 M in Six Locations in Urban Areas

Haryono Setiyo Huboyo*[1], Okto Risdianto Manullang[2], Budi P Samadikun[1]

[1]Department of Environmental Engineering, Diponegoro University

[2]Department of Urban and Regional Planning, Diponegoro University

ARTICLE INFO

ABSTRACT

Several activities in urban areas emit CO_2 gas and the amount of the emission is closely related to land use. This will, in turn, increase global warming phenomena in urban areas. So far, the estimation of pollutant concentrations in the ambient air has been carried out at the height of human breath, and very rarely the concentration values at low-level altitudes have been studied in Indonesia. This study tries to analyze the CO_2 concentration based on different altitudes and different locations.

Measurements of this study were carried out in industrial, residential, commercial, and highway areas using drones at two altitudes of 1.5 m and 15 m. The use of altitude variations to know the homogeneity of CO_2 spatial distribution at different heights. The results of the study showed CO_2 concentrations on weekday mornings and afternoons, and weekend mornings in the sampling areas at 1.5 m and 15 m in the range of 393 – 462 ppm and 391 – 460 ppm, respectively. The statistical test showed that there is no significant CO_2 concentration difference between altitudes of 1.5 m and 15 m, with only a 0.17% difference value on average. The Tugu Industrial Estate area has the highest concentration of CO_2, while the area on Jalan Perintis Kemerdekaan has the lowest concentration.

1. INTRODUCTION

Global warming, whose main source is CO_2 gas emissions, has been studied worldwide by many researchers, and the largest emitter of CO_2 is mainly caused by various human activities (Ahundjanov & Akhundjanov, 2019). Several direct and indirect impacts will occur when the concentration of CO2 gas in the atmosphere is very high (Houghton, J.T., GJ. Jenkins, 2018). Based on current measurements, average global CO_2 concentrations have reached around 417 ppm, which is a 50% increase from the 18th century (Betts, 2021). There are three main factors related to human activities that produce CO_2 emissions, namely the use of buildings, industrial activities, and the increasing number of vehicles for transportation. The nature of the resulting CO_2 emission, which is the main greenhouse gas (GHGs), has a temporal and spatial distribution. In India, based on the data obtained from the monitoring program, it is found that the major contributors are from the industry (Chaudhari et al., 2007). Meanwhile, in 2010 the main contributor to GHGs emissions in Indonesia was the forestry sector (49%), followed by energy use (34%) (KLHK, 2021). Meanwhile, related to energy use in daily activities, the energy use for residential buildings, commercial activities, and office areas is a contributor to GHG emissions in the building sector. The high concentration of CO_2 in the ambient can also affect the

concentration of CO_2 in the indoor air (Kim & Choi, 2019). The high concentration of inhaled CO_2 poses a dangerous risk for indoor occupants (Brown et al., 2017). In addition, Earth's temperature is getting higher due to the increasing amount of CO_2 in the atmosphere (Liu, Waqas, Wang, Xiong, & Wan, 2017). The high temperature on earth is due to the reflection of sunlight energy into space that has reached the earth.

UAVs (Unmanned Aerial Vehicles or drones) equipped with air quality monitoring devices have been widely used to improve monitoring efficiency and accuracy nowadays. With the increasing number of air pollution episodes that need to be handled quickly, UAVs equipped with air monitoring devices are widely used to detect air pollution in various areas (Yao, Wei, Zhang, & Li, 2018). During in situ air quality measurement, UAVs could be equipped with various sensors. Thus making this method more effective and becoming a trend, especially in the study of air quality and climate change (Villa, Gonzalez, Miljievic, Ristovski, & Morawska, 2016). Generally, serial gas sensors and microcontrollers are integrated into the UAV to ensure the implementation of the air quality monitoring system. With this system, measurements of air quality or GHGs can be carried out at various heights according to the operating height of the UAV (Abdelrahman, Balkis, Abou-Elnour, & Tarique, 2018).

Currently, air pollutant monitoring systems using UAVs can be used in a real-time mode so that they can better describe the real conditions at the measurement location. The integration of the sensors in the UAV with the measuring coordinate position on earth can be facilitated by the system's modular design. These tools can be carried simultaneously on the UAV (Gu, R. Michanowicz, & Jia, 2018). However, the use of UAVs for air quality measurements has a weakness, namely the limited flight time because it is limited by the characteristics of the UAV size (rotor size, rotor configuration, diameter) and the weight of the UAV itself (Al-Hajjaji, Ezzin, Khamdan, Hassani, & Zorba, 2017). Therefore, before the experiment, the detector is mounted on a UAV with a position that is minimally disturbed by rotor rotation by being analyzed

based on a Computational Fluid Dynamics (CFD) simulation (Zhou, Peng, Wang, Shen, & Liu, 2018).

Various types of UAVs have been developed, some of which include fixed-wing aircraft, helicopters (chopper), multi-copter, parachute and glider motors, UAVs with vertical take-off landing, assembled UAVs, and commercialized UAVs (Hassanalian & Abdelkefi, 2017). All types are made based on certain interests and have their own advantages and disadvantages. Current UAV implementations include environmental monitoring, traffic management, pollution monitoring, civil security control, and shipping of goods (Mohamed, Al-Jaroodi, Jawhar, Idries, & Mohammed, 2020). Air quality assessments have traditionally been carried out by monitoring land bases with manned aircraft or satellites. To measure the effects of atmospheric pollution on human health and the environment, detailed information about the characteristics of aerosol spatial distribution and pollutant concentration is needed (Peng, Wang, Wang, Gao, & Lu, 2015). However, data from land bases and satellite measurements are relatively sparse and often inadequate in terms of not having enough data to be used for ground-level analysis in the source-receptor study. In addition, satellites and land-based sensors require expensive costs that result in limitations in the analysis. The limitation related to effectively measured spatial aerosol distribution triggers the use of UAVs for atmospheric measurement and monitoring. UAV methods can cover large areas and can monitor locations that are remote, dangerous, or difficult to access, increasing operational flexibility and resolution of land-based methods (Villa et al., 2016). The advantages of UAVs compared to other methods include accuracy, flexibility, flexible height exploration, and continuous data collection (Babaan, Ballori, Tamondong, Ramos, & Ostrea, 2018).

This study aims to analyze differences in CO_2 gas concentrations based on different heights. Six locations were selected for research observation sites which represent industrial, commercial, residential, and transportation areas.
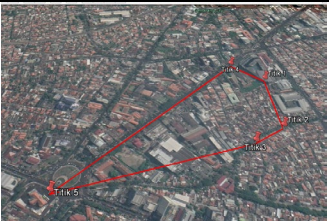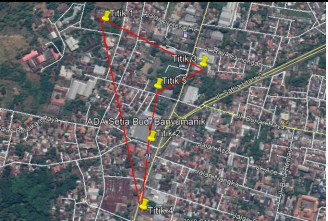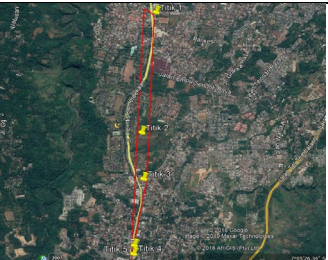
2. METHODS

In this study, 6 different study sites were selected in the city of Semarang, which represent industrial, residential, transportation, and commercial areas. At that six locations, 30 points of CO_2 concentration (each location site has 5 points measurements) were measured and measured at different heights (1.5 m and 15 m). Tugu Industrial Estate in the North-Western Part of Semarang was selected to represent the industrial area. The commercial area includes 2 different locations, namely the Paragon City Mall area and the Ada Swalayan Setiabudi area. Measurement in the housing area took place at Tugurejo Village and housing, Central Semarang. While Perintis Kemerdekaan, as an inter-province connection road, was chosen to represent the use of transportation land. To represent the conditions in the field, measurements were made on weekdays and holidays in the morning and evening. Measurements were carried out in the period 13 July - 22 July 2019. Location details (location description, coordinates, and map) are shown in Table 1.

Sampling was carried out using AZ Instrument China CO_2 meter production with type AZ-7755 which was calibrated with the manufacturing standard (calibrating at 400 ppm standard CO_2). This tool has a reading specification of CO_2 gas concentrations in the numbers 0 to 2000 ppm with an accuracy of ± 5%. CO_2 concentration readings run every second. The response time for measuring CO_2 gas is 30 seconds, with a warm-up time of 30 seconds. Furthermore, CO_2 meters will be installed in the UAV body and flown using a UAV-type DJI Phantom 4 Standard, which has the specifications for the farthest flight range of 3.1 miles with a flying time of 28 minutes. This is a small UAV that has an operating altitude of < 1200 ft and a weight of only 1.38 kg. DJI Phantom 4 is capable of flying with a maximum speed of 44.7 mph. CO_2 measurements were carried out at an altitude of 1.5 m and 15 m with 2 repetitions. Before flying, wait 30 seconds to wait for the CO_2 meter warm-up time. After 30 seconds, the UAV was flown to the first height of 1.5 m and measured for 10 seconds, then to the second height of 15 m and again measured for 10 seconds. Due to the measurement repetition, thus we got 20 measurement events at each point. Thus, the CO_2 concentration data obtained from the measurement results amounted to 40 data with 20 data for each height. The measurement data storage is done by recording the CO_2 meter screen using a UAV camera which is then stored on a microSD.

Table 1. Site Sampling Description

Location	Coordinates	Map	Location	Coordinates	Map
Tugu industrial area	6°58'29.84"-6°57'55.73"S 110°19'31.43"-110°20'5.24"E		Tugurejo residential area	6°59'1.72"-6°59'0.62"S 110°20'39.50"-110°21'20.83"E	
Mall Paragon City area	6°59'4,64"–6°58'56,92" S 110°24'33,04"–110°24'58,02"E		ADA Supermall	7°3'28.88"-7°3'50.53"S 110°24'41.59"-110°24'45.71"E	
Central Semarang residential area	6°59'1,58"–6°59'1,15" S 110°25'9,84"–110°25'33,08"E		Perintis Kemerdekaan road	7°4'36.71"-7°6'8.51"S 110°24'41.65-110°24'33.48"E	
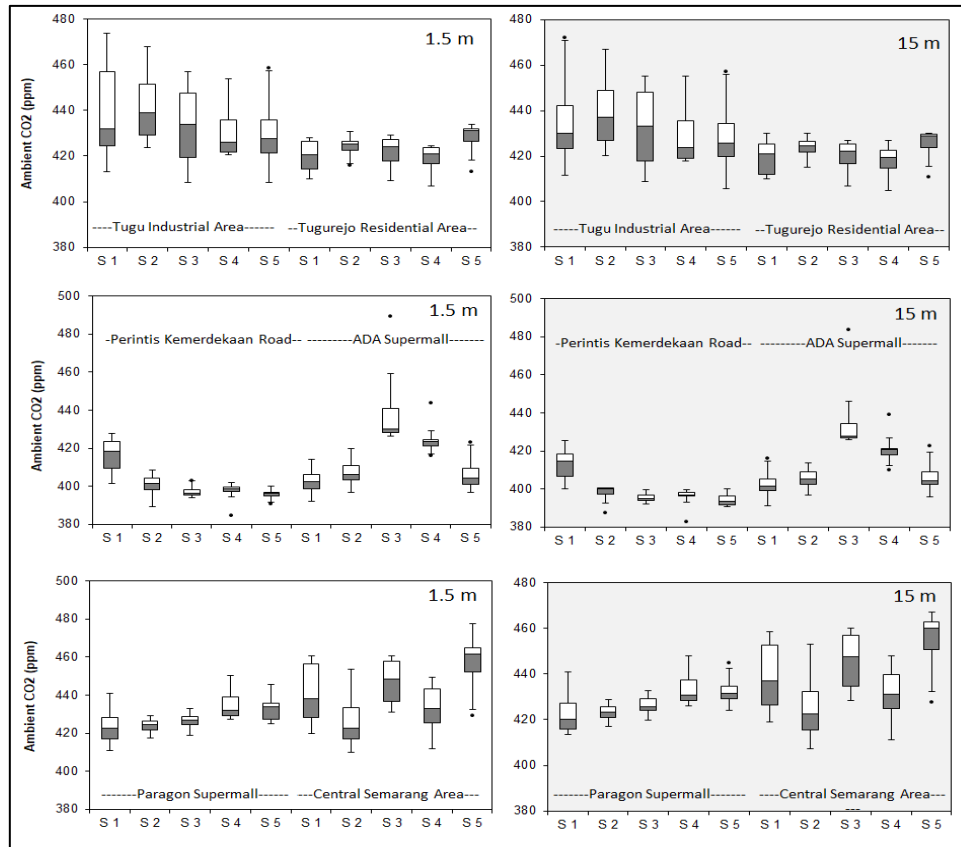
Figure 1. Distribution of CO_2 Concentration at Each Measurement Point on Weekend-Weekday and Morning-Afternoon Conditions

3. RESULTS AND DISCUSSION

Measurements were made during the dry season, so there was no rain during the measurement period. Figure 1 shows the distribution of the measurement results (averaged 10 times measurements) for each location on weekday-weekend and morning-evening conditions for point 1 (S1) to point 5 (S5). Figure 1 revealed that there is a difference in the average concentration between locations, but in one location, there is no difference in the average concentration at the height of 1.5 m and 15 m.

The following Table 2 shows a recapitulation of the measured CO_2 gas results.

Based on table 2, CO_2 concentration from 1.5 m to 15 m height tends to decrease. The condition in which 1.5 m height is closer to the source of emission and gradually gets further until the height of 15 m, altering this reduction of CO_2 concentration. The wind speed ratio at Semarang during the measurement period ranged from 1.34 to 1.37

according to secondary data on wind speed (Figure 2) (Significantly different). Therefore, it was reasonable to predict that the wind speed between 1.5 m and 15 m heights varied significantly. According to Turgut & Usanmaz (2016), the reduction of CO_2 concentration is also caused by wind speeds that increase along with the level of land surface elevation. In line with the results of the study of Tasić, Kovačević, & Milošević (2013), the higher the wind speed, the concentration of gas in the air will be smaller because the gas is carried by the wind away from the measurement location.

To test the assumption above, data on CO_2 concentrations were processed with SPSS analysis. Independent sample T-test revealed that all Sig. (2-tailed) results are more than 0.05. Therefore, it can be said that there is no statistically significant difference between the average CO_2 gas concentration measurements at 1.5 m and 15 m. The significant variation in wind speed had little

impact on CO_2 concentration at these two heights since both locations are presumably too close in the distance. Thus, CO_2 gas concentrations are not significantly different.

It is necessary to know the variation in different CO_2 concentrations at certain altitudes to see the homogeneity of concentrations based on altitude. Furthermore, the Surfer program is used to map the CO_2 distribution to make it easier to describe the spatial distribution. The following Figures represent the distribution of CO_2 concentrations for each measurement location.
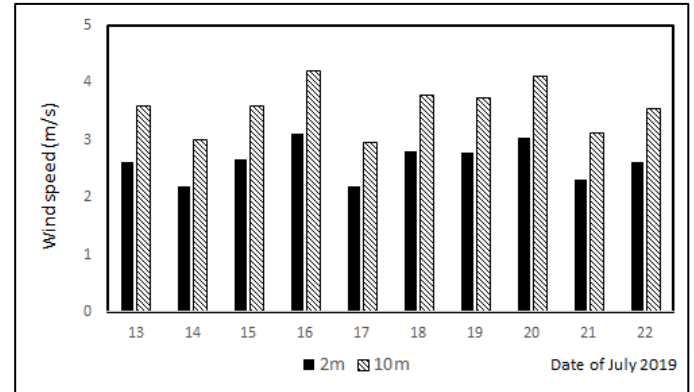
Data taken from NASA USA (NASA, 2022)

Figure 2. Wind Speed at Altitude of 2 m and 10 m

Table 2. Recapitulation of CO_2 Gas Measurement Results

Location	Sampling time	Concentration CO_2 (ppm)						Independent T-Test Sig. (2-tailed)
		Measurement 1			Measurement 2			
		1,5 m	15 m	% reduction	1,5 m	15 m	% reduction	
Tugu industrial area	Weekend Morning	434.42	428.78	1.30	428.56	426.9	0.39	0.254
	Weekend Afternoon	420.18	418.66	0.36	419.46	417.66	0.43	
	Weekday Morning	462.16	460.92	0.27	459.46	458.14	0.29	
	Weekday Afternoon	429.56	428.7	0.20	427.94	426.2	0.41	
Tugurejo residential area	Weekend Morning	427.28	427.76	0.11	427.54	426.8	0.17	
	Weekend Afternoon	426.04	423.9	0.50	425.3	423.58	0.40	
	Weekday Morning	419.54	419.28	0.06	417.58	415.6	0.47	
	Weekday Afternoon	417.18	415.64	0.37	417.6	416.04	0.37	
ADA Supermall	Weekend Morning	411.34	410.34	0.01	405.94	404.96	0.009	0,597
	Weekend Afternoon	408.34	406.24	0.021	408.96	405.58	0.034	
	Weekday Morning	412.72	412.3	0.004	413.46	412.1	0.014	
	Weekday Afternoon	433.86	431.36	0.025	432.2	428.72	0.035	
Perintis Kemerdekaan road	Weekend Morning	398.44	398.06	0.004	393.32	391.6	0.017	
	Weekend Afternoon	404.5	401.44	0.031	404.56	401.54	0.030	
	Weekday Morning	401.46	399.36	0.021	403.64	400.12	0.035	
	Weekday Afternoon	401.62	401.06	0.006	403.86	400.96	0.029	
Mall Paragon City area	Weekend Morning	424,22	422,66	0,016	420,24	421,2	-0,009	0,754
	Weekend Afternoon	426,58	424,68	0,019	423,54	423,1	0,004	
	Weekday Morning	431,9	431,52	0,004	430,98	429,04	0,019	
	Weekday Afternoon	436,34	436,08	0,003	436,3	435,24	0,011	
Central Semarang residential area	Weekend Morning	447,5	445,5	0,02	441,64	441,12	0,005	
	Weekend Afternoon	422,9	420,72	0,022	420,3	418,9	0,014	
	Weekday Morning	457,48	455,92	0,016	454,7	453,52	0,012	
	Weekday Afternoon	441,78	437,4	0,044	438,7	437,62	0,011	

Figure 3 and Figure 4 below show the distribution of CO_2 concentrations in the Tugurejo District and Tugu Industrial Estate.

Figure 3 and Figure 4 revealed that Tugu Industrial Estate had a higher CO_2 concentration than Tugurejo sub-district housing. In comparison to the residential sampling area, Tugu Industrial Estate probably has more pollution-producing sources. The confluence of the road and the railroad line at Tugu Industrial Estate frequently results in traffic bottlenecks during peak hours. In addition, the emission load from factories at Tugu Industrial Estate is also quite large. On the weekend afternoon, however, CO_2 concentrations in Tugu

Industrial estates were lower than Tugurejo Housing. The reduction of industrial activity by all companies in Tugu Industrial Estate during weekend afternoon presumably takes part in this CO_2 concentration drastic decline. Therefore, it can be concluded that the source of emissions came from all activities that support the production process within Tugu Industrial Estate. While the cross-section image of the 3D map shows that the concentration value at an altitude of 1.5 m tends to be higher than the concentration at an altitude of 15 m, the

difference in concentration between altitudes is not significant.

Figure 5 and Figure 6 below show the distribution of CO_2 concentrations in the Commercial Area of the ADA Mall and the Perintis Kemerdekaan Road.

Figures 5 and 6 show that the Commercial Area of the ADA Mall has greater CO_2 concentrations than the Perintis Kemerdekaan Road. This is due to the supermarket's high building density in the commercial area, which results in poor air circulation. Due to its location at the intersection of three major roads—the toll road, Perintis Kemerdekaan Road, and Setiabudi Road—ADA Mall sees a lot of traffic. A high-level emission in this location is also a result of activity in the mall parking lot. These finally led to CO_2 concentration values that were greater than those on Perintis Kemerdekaan road. The findings of CO_2 concentrations in the morning and evening at the same location point are not significantly different, as shown in Figures 5 and 6. However, the CO_2 concentration can vary greatly across these two different sites. In conclusion, rather than having a vertical or temporal distribution, CO_2 gas was distributed spatially.
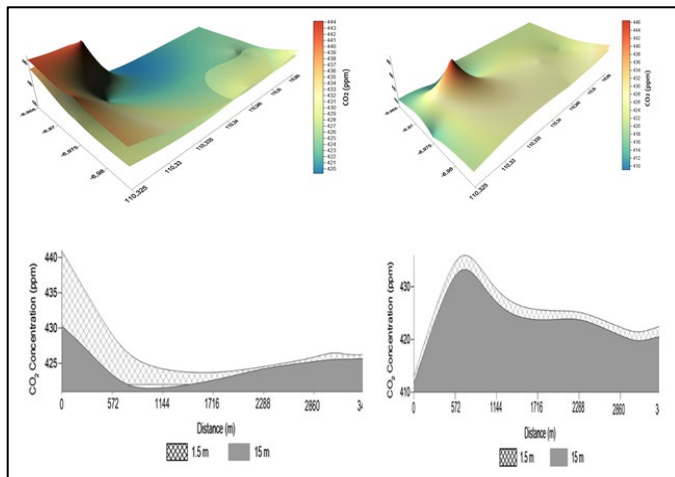
(a) *Weekend* Morning   (b) *Weekend* Afternoon

Figure 3. Map and Cross section of CO_2 Concentration Distribution in Tugu Industrial Estate and Tugurejo Village Housing in Weekend
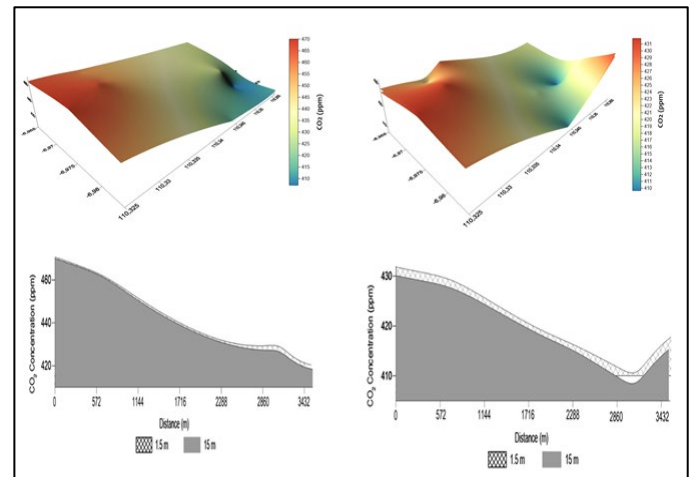
(a) *Weekday* Morning   (b) *Weekday* Afternoon

Figure 4. Map and Cross section of CO_2 Concentration Distribution in the Tugu Industrial Estate and Tugurejo Village Housing on Weekday
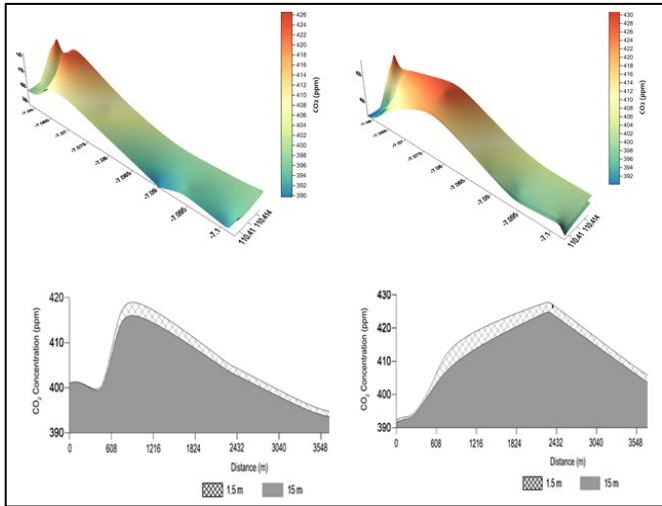
(a) *Weekend* Morning   (b) *Weekend* Afternoon

Figure 5. Map and Cross section of CO₂ Distribution in Commercial Areas. There are Supermarkets and Independence Pioneer Roads on Weekend
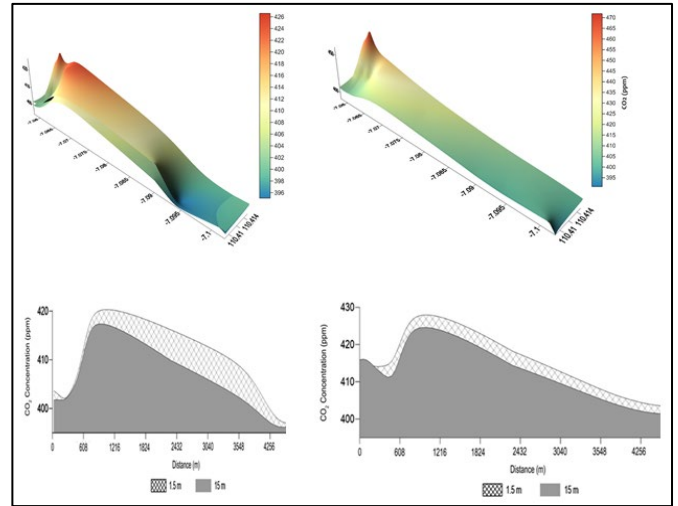
(a) *Weekday* Morning   (b) *Weekday* Afternoon

Figure 6. Map and Cross section of CO₂ Distribution in ADA Mall Commercial Areas and Perintis Kemerdekaan Roads on Weekday
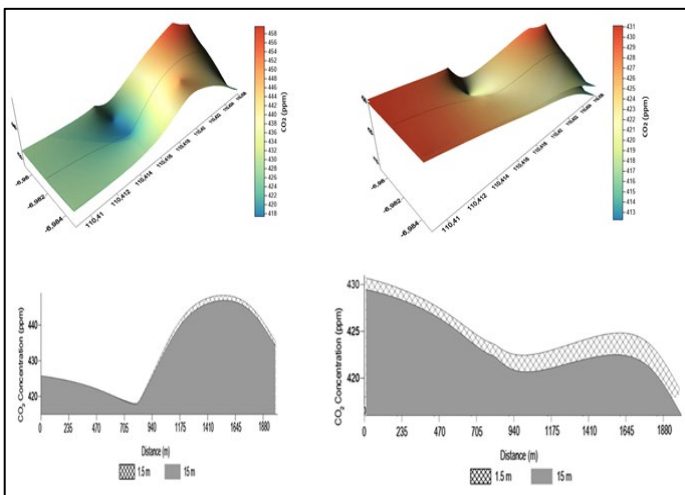
(a) *Weekend* Morning   (b) *Weekend* Afternoon

Figure 7. Map and Cross section of CO₂ Concentration Distribution in Paragon Mall Commercial Area and Housing Around Central Semarang at Weekend
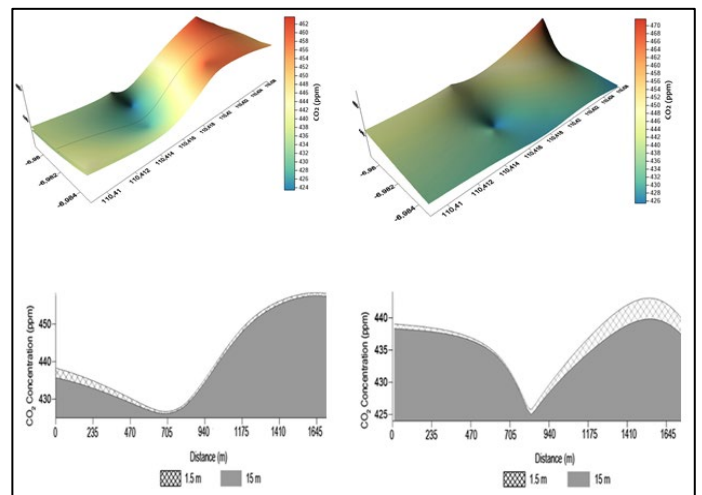
(a) *Weekday* Morning   (b) *Weekday* Afternoon

Figure 8. Map and Cross-section of CO₂ Concentration Distribution in Paragon City Mall Commercial Area and Housing Around Central Semarang on Weekday

The distribution of CO_2 concentrations in the Paragon Mall's commercial area and the housing near Central Semarang is depicted in Figures 7 and 8 below. According to Figures 7 and 8, the Central Semarang Housing area tends to have a higher distribution of CO_2 gas on weekday and weekend mornings, as seen by the significant CO_2 concentration on the right. This is brought on by household and domestic-related activities, as well as high waste disposal that produces additional CO_2 emissions. However, on a Saturday afternoon, the Paragon Mall's commercial area had a greater CO_2 concentration as a result of increased commercial activity, which was reflected in an increase in the number of visitors. According to the cross-section analysis, although there is no significant difference

in concentration between the heights, the concentration at 1.5 m tends to be larger than the concentration at 15 m.

There was no significant difference in CO_2 gas content between 1.5 m and 15 m, per the findings of measurements taken at all six locations. As a result, gas measurements at the height of around 15 m are equivalent to 1.5 m. However, given that they have a larger density than gas, particulates as a contaminant need more study. The fact that there are variations in CO_2 gas content and spatial distribution is another intriguing fact. This suggests that it is important to quantify pollutant concentrations in a more constrained location in order to assess the impact of air pollution on health. This is to prevent inhalation concentration bias in health impact studies due to the spatial distribution of pollutants.

Above all, there are drawbacks in this study where the level of accuracy of the instrument is 5% while the difference in measurement results is <5%, especially those in commercial and residential areas, so the differences that occur are still within the error range of the CO_2 monitor.

4. CONCLUSION

According to the study's results and discussion, we can draw the following conclusions:

1. The results of carbon dioxide (CO_2) gas concentration measurements from 6 regions show that the Industrial area has the highest CO_2 concentration value. Complex sources (transport and industry) influence air pollution, particularly in Tugu Industrial Estate, resulting in higher carbon dioxide (CO_2) gas concentration compared to the other measurement locations.

2. Based on the statistical analysis, there are no significant differences in CO_2 concentrations at 1.5 m and 15 m at any of the measurement sites. Only 0.17 percent, on average, separates the concentration at 1.5 and 15 meters sampling points. However, there are variations in the spatial distribution of CO_2 gas concentration.

Reflecting on the results of this study, measuring gas concentrations in urban areas, where setting up the instrument at the height of human breath is constrained by the location condition, then measurements at an altitude of up to 15 m instead of 1.5 m above ground are still feasible

to be done. Further research is needed to determine whether the particulate parameters at the height of 15 m could be done similarly.

5. ACKNOWLEDGMENT

6. REFERENCE

Abdelrhman, M., Balkis, A., Abou-Elnour, A., & Tarique, M. (2018). Environmental Monitoring System by Using Unmanned Aerial Vehicle. *Network Protocols and Algorithms*, *9*, 31. https://doi.org/10.5296/npa.v9i3-4.12021

Ahundjanov, B. B., & Akhundjanov, S. B. (2019). Gibrat's law for CO_2 emissions. *Physica A: Statistical Mechanics and Its Applications*, *526*, 120944. https://doi.org/10.1016 /j.physa.2019.04.180

Al-Hajjaji, K., Ezzin, M., Khamdan, H., Hassani, A. El, & Zorba, N. (2017). Design, Development and Evaluation of a UAV to Study Air Quality in Qatar. *ArXiv, abs/1709.0*.

Babaan, J. B., Ballori, J. P., Tamondong, A. M., Ramos, R. V., & Ostrea, P. M. (2018). Estimation of PM 2.5 vertical distribution using customized UAV and mobile sensors in Brgy. UP Campus, Diliman, Quezon City. *International Archives of the Photogrammetry, Remote Sensing and Spatial Information Sciences - ISPRS Archives*, *42*(4/W9), 89–103. https://doi.org/10.5194/isprs-archives-XLII-4-W9-89-2018

Betts, R. (2021). Met Office: Atmospheric CO_2 now hitting 50% higher than pre-industrial levels. Retrieved June 28, 2022, from https://www.carbonbrief.org/met-office-atmospheric-co2-now-hitting-50-higher-than-pre-industrial-levels/

Brown, A., Eickhoff, C., Reinders, J. E. A., Raben, I., Spruijt, M., & Neele, F. (2017). IMPACTS:

Framework for Risk Assessment of CO_2 Transport and Storage Infrastructure. *Energy Procedia, 114,* 6501–6513. https://doi.org/https://doi.org/10.1016/j.egypro.2017.03.1786

Chaudhari, P. R., Gajghate, D. G., Dhadse, S., Suple, S., Satapathy, D. R., & Wate, S. R. (2007). Monitoring of environmental parameters for CO_2 sequestration: a case study of Nagpur City, India. *Environmental Monitoring and Assessment, 135*(1–3), 281–290. https://doi.org/10.1007/s10661-007-9649-7

Gu, Q., R. Michanowicz, D., & Jia, C. (2018). Developing a Modular Unmanned Aerial Vehicle (UAV) Platform for Air Pollution Profiling. *Sensors, 18*(12). https://doi.org/10.3390/s18124363

Hassanalian, M., & Abdelkefi, A. (2017). Classifications, applications, and design challenges of drones: A review. *Progress in Aerospace Sciences, 91*(November 2016), 99–131. https://doi.org/10.1016/j.paerosci. 2017.04.003

Houghton, J.T., GJ. Jenkins, J. J. E. (2018). ipcc_far_wg_I_ full_report.pdf. *Climate Change.*

Kim, M. K., & Choi, J.-H. (2019). Can increased outdoor CO_2 concentrations impact on the ventilation and energy in buildings? A case study in Shanghai, China. *Atmospheric Environment, 210,* 220–230. https://doi.org/https://doi.org/10.1016/j.atmosenv.2019.04.015

KLHK. (2021). *Updated Nationally Determined Contribution Republic of Indonesia 2021.*

Liu, S., Waqas, M. A., Wang, S. H., Xiong, X. Y., & Wan, Y. F. (2017). Effects of increased levels of atmospheric CO_2 and high temperatures on rice growth and quality. *PLoS ONE, 12*(11), 1–15. https://doi.org/ 10.1371/journal.pone.0187724

Mohamed, N., Al-Jaroodi, J., Jawhar, I., Idries, A., & Mohammed, F. (2020). Unmanned aerial vehicles applications in future smart cities. *Technological Forecasting and Social Change, 153,* 119293.

ttps://doi.org/https://doi.org/10.1016/j.techfore.2018.05.004

NASA. (2022). POWER | Data Access Viewer. Retrieved June 26, 1BC, from https://power.larc.nasa.gov/data-access-viewer/

Peng, Z.-R., Wang, D., Wang, Z., Gao, Y., & Lu, S. (2015). A study of vertical distribution patterns of PM2.5 concentrations based on ambient monitoring with unmanned aerial vehicles: A case in Hangzhou, China. *Atmospheric Environment, 123.* https://doi.org/ 10.1016/j.atmosenv.2015.10.074

Tasić, V., Kovačević, R., & Milošević, N. (2013). Investigating the impacts of winds on SO2 concentrations in Bor, Serbia. *Journal of Sustainable Development of Energy, Water and Environment Systems, 1*(2), 141–151. https://doi.org/10.13044/j.sdewes.2013.01.0010

Turgut, E. T., & Usanmaz, Ö. (2016). An Analysis of Altitude Wind and Humidity based on Long-term Radiosonde Data. *ANADOLU UNIVERSITY JOURNAL OF SCIENCE AND TECHNOLOGY A - Applied Sciences and Engineering, 17*(5), 830–830. https://doi.org/10.18038/aubtda.279852

Villa, T. F., Gonzalez, F., Miljievic, B., Ristovski, Z. D., & Morawska, L. (2016). An Overview of Small Unmanned Aerial Vehicles for Air Quality Measurements: Present Applications and Future Prospectives. *Sensors, 16*(7). https://doi.org/ 10.3390/s16071072

Yao, Y., Wei, S. Y., Zhang, H., & Li, Q. (2018). Application of UAV in Monitoring Chemical Pollutant Gases.

Zhou, S., Peng, S., Wang, M., Shen, A., & Liu, Z. (2018). The Characteristics and Contributing Factors of Air Pollution in Nanjing: A Case Study Based on an Unmanned Aerial Vehicle Experiment and Multiple Datasets. *Atmosphere, 9*(9). https://doi.org/10.3390/ atmos9090343

Evaluation of the Implementation Integrated Biological System Industrial Wastewater Treatment Plant: Pollutant Removal, Operational Maintenance, Estimation of Carbon Emission

Nanik Indah Setianingsih*[1], Agus Purwanto[2], Farida Crisnaningtyas[2], Ikha Rasti Julia Sari[2]

[1]National Research and Innovation Agency

[2]Center for Standardization and Industrial Pollution Prevention Services

ABSTRACT

The development of WWTP in business activities needs to pay attention to getting appropriate WWTP that is more valuable to support sustainable development. This study aims to evaluate two systems of integrated biological WWTP; anaerobic-wetland, and anaerobic-aerobic-wetland, including the effectiveness of pollutant removal, operational and maintenance, and estimation of carbon emissions. The performance of pollutant removal was evaluated by analyzing inlet and outlet samples of WWTP. An operational and maintenance evaluation was carried out by studying the WWTP operating system and maintenance procedures supported by a literature review. Carbon emission estimation was carried out using a formula referring to the IPCC Guidelines (2006). Organic matter removal of anaerobic-aerobic-wetland WWTP in the form of BOD_5 and COD are 92.12% and 91.72%, respectively, higher than anaerobic-wetland WWTP are 88.69% of BOD_5 and 77.62% of COD. Anaerobic-aerobic-wetland WWTP needs more maintenance and operation than anaerobic-wetland WWTP. The highest carbon emission of both WWTP is 41530.91 $kgCO_2$ eq/year of anaerobic-wetland WWTP from the organic matter removal process and 46485.15 $kgCO_2$ eq/year of anaerobic-aerobic-wetland WWTP. Electrical energy consumption emits in anaerobic-aerobic-wetland WWTP is 22338 $kgCO_2$ eq/year higher than anaerobic-wetland WWTP at 4299.70 $kgCO_2$ eq/year. Total carbon emissions of anaerobic-wetland WWTP is 47404.58 $kgCO_2$ eq/year and anaerobic-aerobic-wetland WWTP is 68900.23 $kgCO_2$ eq/year.

1. INTRODUCTION

Water and Sanitation Hygiene (WASH) is one of the crucial things to be concerned about in the world due to climate change. WASH climate-resilient development is one of the programs in realizing the Sustainable Development Goals, one of which is the construction of WASH facilities such as wastewater treatment plants (WWTP) to treat domestic and industrial wastewater. In Indonesia, the Government has required the treatment of industrial and domestic wastewater generated from every business activity as stated in the Minister of Environment Regulation No. 68 of 2016 and P.16/Menlhk/Setjen/Kum.1/4/2019.

The development of WWTP in business activities needs to pay attention to some criteria, including selecting the right technology to treat pollutants in wastewater, investment and operational costs, the presence of by-products, and the carbon emissions generated from the wastewater treatment process. The appropriate WWTP will be more economically valuable and encourage WWTP operations' sustainability to support sustainable development.

Domestic and industrial wastewater generally contains high amounts of organic substances that potentially emit carbon emissions. Therefore, several technologies have been applied in treating both industrial and domestic WWTP wastewater there are chemical-physical (Mukimin et al., 2017; Vistanty et al., 2015; Crisnaningtyas and Vistanty, 2016), aerobic-anaerobic treatment (Yuliasni et al., 2017; Novarina et al., 2020), and wetlands (Moenir et al., 2014; Marlena et al., 2018).

In order to support the achievement of climate resilience, the selection of WWTP technology should follow the Climate Smart-WASH Technology criteria in the IPCC (2006). Furthermore, not only effective in degrading pollutants in wastewater, but the operated WWTP should also have minimum carbon emissions that lead to the least possible impact on climate change.

Biological WWTP can be an effective option in the treatment of wastewater from business activities, both industrial and domestic wastewater. In full-scale application, integrated biological technology has been applied to meet the requirement effluent standard (Setianingsih et al., 2021). One of the advantages is an integrated biological system capable of treating the combined wastewater (Setianingsih et al., 2020). In operation, biological WWTP is fewer chemicals than physical-chemical WWTP and does not discharge toxic & hazardous by-products (Ng. et al., 2014; Marlena et al., 2016). On the other hand, biological WWTP potentially produce carbon emissions. Therefore, the evaluation of implemented WWTP is needed to determine the effectiveness and impact on the environment to achieve the right technology in wastewater treatment. This study aims to evaluate two systems of integrated biological WWTP, including the effectiveness of pollutant removal, operational and maintenance, and estimation of carbon emissions for supporting the improvement of sustainable development and reducing global warming.

2. METHODS

This research evaluated two systems integrated biological WWTP implemented in the industrial sector, PT. Reckitt Benckiser and Hotel Griya Persada; both wastewater treatment plants treat domestic wastewater. However, the domestic activities of PT. Reckitt Benckiser are bathroom activities, washing, and ablution, whereas the domestic activities of Hotel Griya Persada are bathroom activities, washing, catering, and ablution. Furthermore, the system of WWTP implemented at PT. Reckitt Benckiser consisted of anaerobic-wetland. Meanwhile, the system of WWTP at Hotel Griya Persada consisted of anaerobic-aerobic-wetland. The evaluation of the WWTP system is carried out by analyzing several categories, including the performance of pollutant removal, operational and maintenance of WWTP, and estimation of carbon emissions.

2.1. Performance of removal pollutant

Evaluation of pollutant removal performance was carried out of two WWTP systems by analyzing inlet and outlet samples of the WWTP with the same wastewater parameters, including pH, BOD_5, COD, TSS, oil & grease, total coliform, and MBAS.

2.2. Operational dan maintenance of WWTP

The WWTP operational and maintenance evaluation was carried out by studying the WWTP operating system and maintenance procedures, including supporting units and equipments, control parameters, the potency of by-products, additives in operational, energy use, and supported by a literature review of several biological WWTP applications.

2.3. Carbon emission estimation

Carbon emission estimation was carried out using a formula referring to the Guidelines for National Greenhouse Gas Inventories (IPCC, 2006). The primary data used were debit, organic matter removal, time of energy use, and BOD_5 effluent. Calculation of carbon emissions from the wastewater treatment sector using the IPCC Guidelines 2006 method is formulated as follows:

2.3.1. Calculation of carbon emissions from wastewater treatment processes

$$Emission \ CH_4 \left(\frac{kgCO_2eq}{year}\right) = Q \times (organic \ matters_{removed}) \times EF \times GWP_{CH_4} \times 365 \ day \ GWP_{CH_4} = 25 \quad (1)$$

$$EF = 0.131 \ kgCH_4/kgCOD_{removed} \quad (2)$$

$$TCOD : TBOD \ ratio \ (Blackwater \ and \ Combined \ Wastewater) : 2.5 : 1 \quad (3)$$

$$EF \ NO_2 = 0.16 \ kg \ N_2O - N/kgN \quad (4)$$

2.3.2. Calculation of carbon emissions from the use of electrical energy

$$Emission \ CO_2 \left(\frac{kgCO_2eq}{year}\right) = watt \times hour \times EFCO_2 \times 10^{-3} \times 365 \ day \quad (5)$$

$$EFCO_2 = 0.5 \ kgCO_2eq/kWh \quad (6)$$

2.3.3. Calculation of carbon emissions from the effluent

$$Emission \ CH_4(kgCO_2eq/year) = Q \times BOD_{eff} \times EF \times GWP_{CH_4} \times 365 \ day \quad (7)$$

$$Emission \ N_2O(kgCO_2eq/year) = Q \times 1N_{eff} \times EF \times \left(\frac{44}{28}\right) \times GWP_{N_2O} \times 365 \ day \quad (8)$$

$$GWP_{N_2O} = 298 \quad (9)$$

$$EF : 0.06 \ kgCH_4/kgCOD_{removed} \ and \ 0.005 \ kg \ N_2O - N/kgN \quad (10)$$

2.3.4. Calculation of carbon emissions from sludge

$$Emission \ CH_4(kgCO_2eq/year) = fS_{removed} \times fS_{volume} \times EF \times GWP_{CH_4} \times 10^{-6} \times 365 \ day \quad (11)$$

Annotation

Q: flow rate of wastewater

EF: emission factor

Total carbon emissions from wastewater treatment systems are (1+2+3+4) kg CO$_2$eq/year.

3. RESULT AND DISCUSSION

3.1. Performance of removal pollutant

The wastewater treatment plant evaluated in this study is an integrated biological system. In full-scale application, the integrated system of several treatment units is mainly applied (Tianzhi et al., 2021) to effectively achieve pollutant removal and meet the required quality standards (Kozak, Cirik, & Başak, 2021). Therefore, an analysis of pollutant removal performance was carried out to determine the ability of the WWTP system to degrade pollutants contained in wastewater. The results of performance evaluation of anaerobic-wetland and anaerobic-aerobic-wetland WWTP in degrading pollutants can be seen in table 1 and table 2.

Table 1. Performance of removal pollutant of anaerobic-wetland WWTP

No	Parameter	analysis result		%
		Inlet	Outlet	Removal
1	BOD$_5$	115	13	88.69
2	COD	240	53.7	77.62
3	TSS	66	9	86.36
4	Oil & grease	<2.38	<2.38	-
5	Total Coliform	16000	240	98.5
6	MBAS	0.8	<0.07	91.25
7	pH	7.1	7.4	

Table 2. Performance of removal pollutant of anaerobic-aerobic-wetland WWTP

No	Parameter	analysis result		%
		Inlet	Outlet	Removal
1	BOD$_5$	184.3	14.52	92.12
2	COD	267.3	22.12	91.72
3	TSS	68	12	82.35
4	Oil & grease	20.21	3.99	80.25
5	Total Coliform	18000	0	100
6	MBAS	1.845	0.211	88.56
7	pH	5.7	7.1	

Table 1 and table 2 inform that the pollutant concentration of inlet wastewater treated in anaerobic-aerobic-wetland WWTP is higher in values for BOD$_5$, COD, TSS, and total coliform parameters than in anaerobic-wetland WWTP. For oil & grease and MBAS parameters, the pollutant concentration in the inlet sample of anaerobic-aerobic-wetland WWTP is much higher and has lower pH than the inlet sample of anaerobic-wetland WWTP. It is because, in anaerobic-aerobic-wetland WWTP, wastewater is generated from domestic activities consisting of bathroom activities, washing, ablution, and catering. Meanwhile, in anaerobic-wetland WWTP, wastewater is generated from bathroom activities, washing, and ablution only, so the value of pollutant concentration is low. Catering activity releases pollutants from food waste and dish soap that increase the concentration of COD, oil & grease, and MBAS (Doma et al., 2014). A high concentration of an organic pollutant from catering activity also affects the pH of inlet wastewater which tend to be low. The effectiveness of pollutant removal of both WWTP systems can be seen in figure 1.

Figure 1 shows the performance of WWTP systems in degrading pollutants in wastewater. Anaerobic-aerobic-wetland system has a higher percentage of BOD$_5$, COD, and Coliform removal than the anaerobic wetland system, which is more than 90%. For TSS and MBAS parameters, the anaerobic-wetland WWTP system has higher performance. In the anaerobic-aerobic-wetland system,

large amounts of organic matter are degraded in two stages, under anaerobic and aerobic conditions (Novarina et al., 2020; Himanshu, 2011), while in the anaerobic-wetland system, organic matter only degraded at anaerobic condition.

Most wetland units degrade nutrient-type pollutants such as ammonia, phosphorus, and residual organic substances from previous processing (Geovana et al., 2016; Moenir et al., 2014; Marlena et al., 2018; Setianingsih et al., 2021). However, the high concentration of oil & grease pollutants and MBAS will be more effectively degraded under aerobic conditions (Primasari et al., 2011). In addition, the presence of MBAS pollutant-containing surfactants is also toxic for anaerobic microbes, so it cannot be optimally treated anaerobically and must be degraded in an aerobic mechanism (Tan, K.N., 2019). The concentration of MBAS in inlet Griya Persada WWTP is higher than in inlet PT. Reckitt Benckiser which needs an aerobic unit to treat optimally.
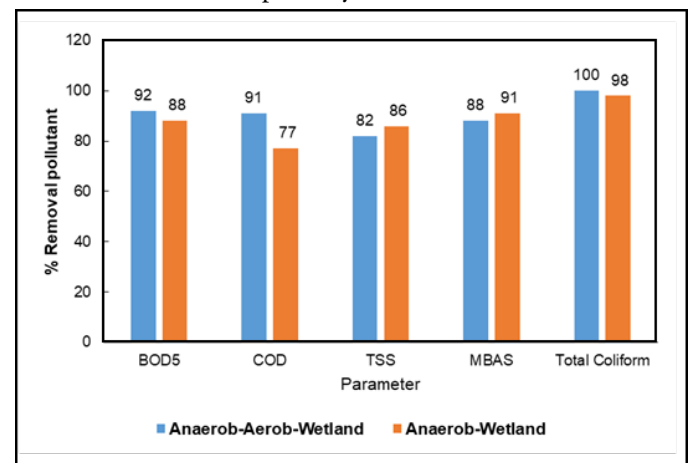
Figure1. Removal pollutant performance of wastewater treatment plant

3.2. Operational maintenance

Operational and maintenance evaluation of WWTP systems was carried out on some properties, as shown in table 3.

In table 3 can be seen that the WWTP system with an aerobic unit generally requires additional units, including a clarifier to settle the sludge and a drying bed to dry the excess sludge. In addition, aerobic WWTP also needs an aerator/blower to supply oxygen for microbes. Therefore,

macronutrients and micronutrients are needed for both WWTP systems. The potency of by-products in the form of sludge in WWTP with the aerobic unit is higher than in WWTP with the anaerobic unit. In conventional aerobic systems, microbial growth is high with the excess sludge reaching 30-50 percent which needs high handling costs (Wei, Y. et al., 2003).

The main control in the operation of biological WWTP is to specify wastewater flows regularly and maintain that there is no obstacle in the pipeline. The aerobic unit will be more controlled and maintained in biological WWTP. Due to aerobic microbial depending on oxygen availability, the amount of dissolved oxygen and

sludge volume index must always be controlled in addition to pH and MLSS in WWTP with an aerobic unit. Dissolved oxygen in the WWTP system with an aerobic unit must be maintained at 2 - 5 mg/L (Du, X. et al., 2018). Lack of oxygen in the WWTP aerobic system will cause negative impacts such as filamentous and bulking sludge (Martins, A.M.P, et al., 2004; D'Antoni, B.M et al., 2017). For the last operation, the energy use of the WWTP system with an aerobic unit will tend to be higher because it requires an additional aerator/blower to supply oxygen for aerobic microbes up to 1.09 kWh/m³ wastewater (Ranieri et al., 2021).

Table 3. Operational and maintenance evaluation of WWTP

No.	Properties	WWTP System		Ref
		Anaerobic-Aerobic-Wetland	Anaerobic-Wetland	
1	Additional units	Clarifier, drying bed	-	Seghezzo, L., 2004; Mulas, M. et al., 2016; Chen et al 2019
2	Equipments	Pump, blower/aerator	Pump	Seghezzo, L., 2004; Mulas, M. et al., 2016; Chen et al 2019
3	Additives	Macro&micro nutrient	Macro&micro nutrient	Seghezzo, L., 2004; Mulas, M. et al., 2016; Chen et al 2019
4	The potency of by-product sludge	Up to 50% in dried condition	10% in thicked condition	Seghezzo, L., 2004; Mulas, M. et al., 2016; Chen et al 2019
5	Control parameters	pH, Dissolved oxygen, MLSS, sludge volume index	pH, MLSS	Seghezzo, L., 2004; Mulas, M. et al., 2016; Chen et al 2019
6	Energy use	*1.09 kWh/m³*	*0.53 kWh/m³*	Seghezzo, L., 2004; Mulas, M. et al., 2016; Chen et al 2019, Ranieri et al., 2021

3.3. Carbon emission estimation

Domestic and industrial wastewater are sources of GHG emissions included in the GHG emission inventory from waste management activities according to the categories stated in the 2006 IPCC Guideline. According to Bappenas (2014), emission reductions from the waste sector have been reported by 11 provinces in Indonesia through main and supporting activities, one of which is the construction of a Wastewater Treatment Plant (WWTP). In this study, the estimation of carbon emissions in the

WWTP system was carried out at the highest pollution load during the operation of WWTP.

3.4. Carbon emission estimation of anaerobic-wetland WWTP

WWTP implemented at PT. Reckitt Benckiser was constructed with a biological system consisting of UASB anaerobic, up-flow anaerobic, and wetland, as shown in figure 2.

The energy requirement for operational WWTP comes from 1 unit of an influent pump with an operating time of 16 hours/day, 1 unit of circulation pump anaerobic, and 1 unit of circulation pump of wetland with an operating time of 24 hours/day. Influent COD was 720.0 mg/L, Effluent COD was 25.14 mg/L, and Effluent BOD_5 was 12.43 mg/L. The anaerobic-wetland system does not produce by-products in the form of sludge. Therefore, the calculation of carbon emissions from sludge management could be ignored. Calculation of carbon emissions for 50 m3/day wastewater treatment with an anaerobic-wetland system as shown in table 4, table 5, and table 6.
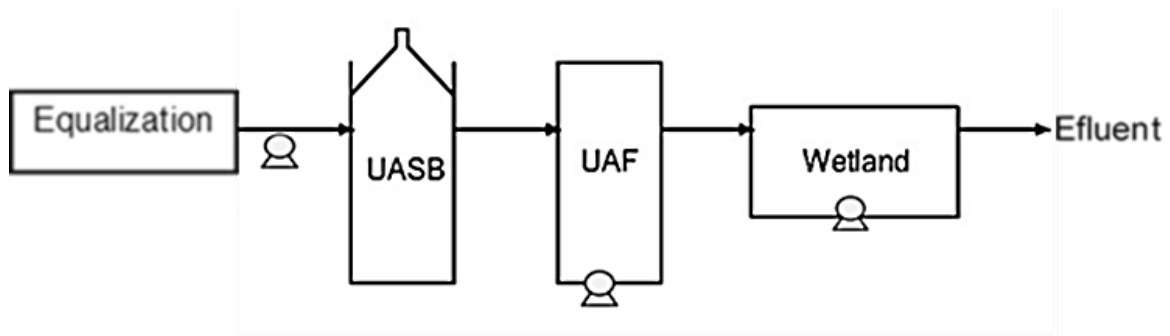
Figure 2. Anaerob-wetland WWTP system

Table 4. Carbon emissions from the wastewater treatment process

Flow rate Q (m³/day)	COD (kg/m³)	EF (kg CH₄/kg COD_removed)	GWP CH₄	Time (day)	Carbon Emission (kgCO₂eq/year)
50	0.69486	0.131	25	365	41530.91

Table 5. Carbon emissions from the use of electrical energy

Equipment	Electrical power (Watt)	Operational time (hour)	EF (kg CO₂)	Conversion factor	Time (day)	Carbon emission (kgCO₂eq/year)
Distribution pump	845	16	0.5	0.001	365	2467.40
Circulation pump I	400	24	0.5	0.001	365	1752
Circulation pump II	300	24	0.5	0.001	365	1314
Total						4299.70

Table 6. Carbon emissions from effluent

Flow rate Q (m³/day)	BOD₅ (kg/m³)	EF (kg CH₄/kg BOD₅ₑff)	GWP CH₄	Time (day)	Carbon emission (kgCO₂eq/year)
50	0.01243	0.06	25	365	340.27

Total carbon emission of anaerobic-wetland WWTP: 47404.58 kgCO₂ eq/year

3.5.   Carbon emission estimation of anaerobic-aerobic-wetland WWTP

WWTP was implemented at Hotel Griya Persada, constructed with a biological system consisting of anaerobic, aerobic, and wetland units. The energy requirement for WWTP operational process comes from 1 unit influent pump, 1 unit anaerobic circulation pump, 1 unit wetland circulation pump, 1 unit clarifier circulation pump, and two unit blowers with an operating time of 24 hours/day. Influent COD was 798.4 mg/L, effluent COD was 20.65 mg/L and effluent BOD was 2.816 mg/L. Sludge in the aerobic unit is circulated with no excess microbial growth. Therefore, the calculation of carbon emissions from the sludge management element could be ignored. Anaerobic-aerobic-wetland WWTP system is shown in figure 3.

Calculation of carbon emissions for 50 m3/day wastewater treatment with an anaerobic-aerobic-wetland system as shown in table 7, table 8, and table 9. Total carbon emission of anaerobic-aerobic-wetland WWTP: 68900.23 $kgCO_2$ eq/year

In biological WWTP, the source of carbon emissions comes from the anaerobic treatment. Aerobic treatment of activated sludge does not release carbon emissions but produces sludge that needs to be processed through anaerobic digestion, land disposal, and incineration. According to Purwanta W and Susanto JP. (2009), greenhouse gas emissions from waste handling activities, including methane (CH_4), nitrous oxide (N_2O), and carbon dioxide (CO_2), occurred under anaerobic conditions. The biological WWTP system used in this research does not produce sludge. Carbon emissions are estimated in wastewater treatment, electrical energy use, and WWTP effluent. Total emissions generated from each source are shown in figure 4.
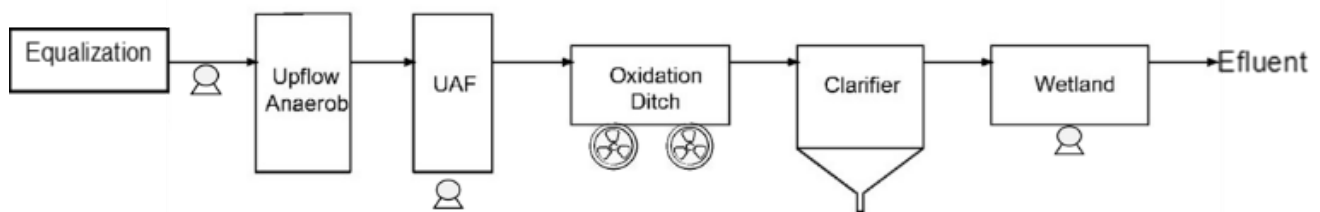
Figure 3. Anaerobic-aerobic-wetland WWTP system

Table 7. Carbon emissions from the wastewater treatment process

Flow rate Q (m³/day)	COD (kg/m³)	EF (kg CH_4/kg $COD_{removed}$)	GWP CH_4	Time (day)	Carbon emission ($kgCO_2$eq/year)
50	0.77775	0.131	25	365	46485.15

Table 8. Carbon emissions from the use of electrical energy

Equipment	Electrical power (Watt)	Operational time (hour)	EF (kg CO_2)	Conversion factor	Time (day)	Carbon emission ($kgCO_2$eq/year)
Circulation pump I	400	24	0.5	0.001	365	1752
Circulation pump I	400	24	0.5	0.001	365	1752
Circulation pump I	400	24	0.5	0.001	365	1752
Distribution pump	900	24	0.5	0.001	365	3942
Blower I	1500	24	0.5	0.001	365	6570
Blower II	1500	24	0.5	0.001	365	6570
Total						22338

Table 9. Carbon emissions from effluent

Flow rate Q (m³/day)	BOD$_5$ (kg/m³)	EF (kg CH$_4$/kg BOD$_{5eff}$)	GWP CH$_4$	Time (day)	Carbon emission (kgCO$_2$eq/year)
50	0.002816	0.06	25	365	77.09
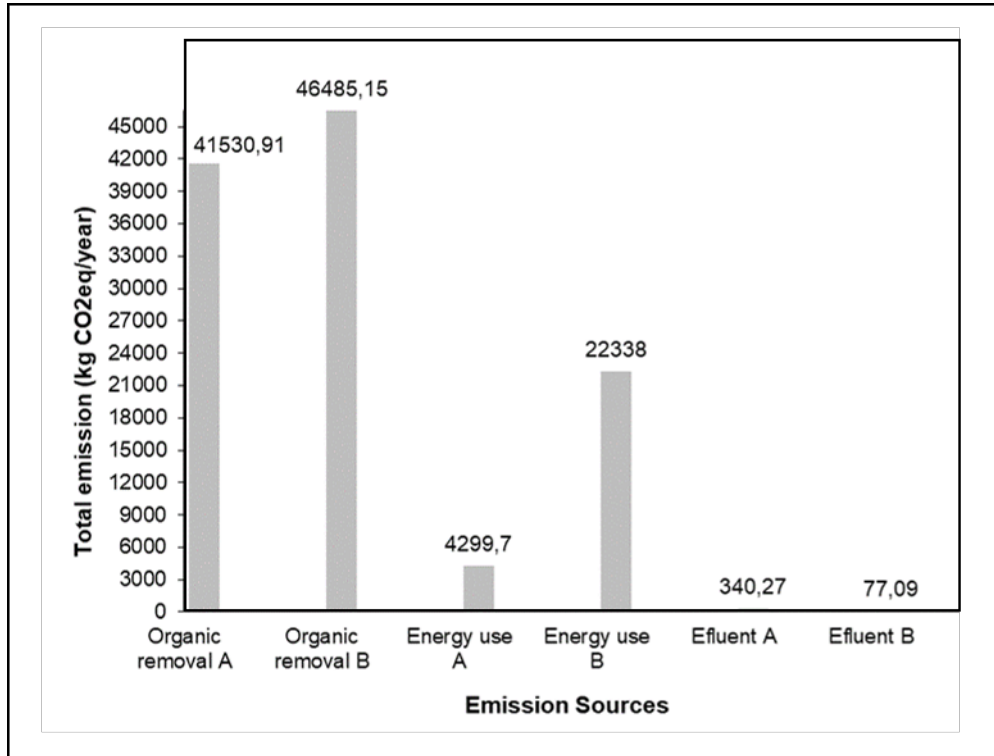
Figure 4. Carbon emission of WWTP system (A) anaerobic-wetland WWTP and (B) anaerobic-aerobic-wetland WWTP

Based on the calculation results, the total carbon emissions of anaerobic-wetland WWTP is 47404.58 kgCO$_2$ eq/year to treat 50 m3/day wastewater with COD influent 720.0 mg/L. Meanwhile, the total carbon emission of anaerobic-aerobic-wetland WWTP is 68900.23 kgCO$_2$ eq/year to treat 50 m3/day wastewater with COD influent 798.4 mg/L. The effluent from both WWTP systems meets the required quality standard with COD below 100 mg/L (Minister of Environment Regulation 2016 and 2019)

In wastewater treatment, anaerobic-wetland WWTP produces emissions of 41530.91 kgCO$_2$ eq/year, while anaerobic-aerobic-wetland WWTP produces emissions of 46485.15 kgCO$_2$ eq/year. The amount of organic matter removal determines carbon emissions in wastewater treatment. Using electrical energy, anaerobic-wetland WWTP releases emissions of 4299.70 kgCO$_2$ eq/year, while anaerobic-aerobic-wetland WWTP releases

emissions of 22338 kgCO$_2$ eq/year. In anaerobic-wetland WWTP effluent releases emissions of 340.27 kgCO$_2$ eq/year and anaerobic-aerobic-wetland WWTP produces emissions of 77.09 kgCO$_2$ eq/year.

The calculated data shows that the highest emissions from both WWTP systems are generated from the wastewater treatment process, and most of the organic matter is degraded in the anaerobic process as the primary unit in the WWTP system. Anaerobic-aerobic-wetland WWTP also emits relatively high emissions in terms of electrical energy consumption due to the use of a blower to supply oxygen for the aerobic system. The electrical energy generated from burning fossil fuels and producing emissions in the form of CO_2 and N_2O also produces (non-CO_2) GHG precursor gases such as CO, CH4, and non-methane volatile organic compounds (NMVOC). These compounds

will be oxidized to CO_2 and gases of N_2O, NOx, NH_3, and SO_2 (Anies et al., 2016).

Carbon emissions have been estimated on black domestic wastewater treatment systems (WASHdev, 2020). Using a conventional anaerobic system, Black domestic wastewater treatment produces emissions of 6046 $kgCO_2$ eq/year for 0.2 m3/day of wastewater. This value will be much higher when compared to carbon emissions in the same volume of wastewater discharged from the implementation of both WWTP systems in this study because the characteristics of wastewater affect the number of carbon emissions. Removal of organic matter in the treatment of domestic black wastewater reaches 3373.92 mg/L, much higher than the removal of organic matter in the studied WWTP system, which is 690 - 770 mg/L.

4. CONCLUSION

Anaerobic-aerobic-wetland WWTP performs higher removal of organic matter than anaerobic-wetland in the form of BOD_5 and COD for 50 m3 volume wastewater. Anaerobic-aerobic-wetland WWTP needs more maintenance and operation of an additional unit, equipment, additive, potency of sludge by-product, control parameters, and energy use than anaerobic-wetland WWTP. Carbon emission from wastewater treatment activities is influenced by the type of biological WWTP system and the level of degradation wastewater. The highest carbon emission of both WWTP resulted from the organic matter removal process, followed by electrical energy consumption and emission from effluent. For 50 m3 volume wastewater, anaerobic-wetland WWTP releases total carbon emissions of 47404.58 $kgCO_2$ eq/year lower than anaerobic-aerobic-wetland WWTP 68900.23 $kgCO_2$ eq/year.

REFERENCES

Anies Ma'rufatin, Wahyu P., Iif M.I., Diyono, Hari S. (2016). Teknologi Pengukuran Emisi Karbon Sektor Limbah. Annual Report-Pusat Teknologi Lingkungan

Bappenas. (2014). Dua Tahun Pelaksanaan RAN-GRK Dan RAD-GRK. Laporan Ringkas

Chen, X., Artur T.M., Kirsten H., Mikkel H.A., Dines T., Gürkan S. (2019). Assessment of Full-Scale N_2O Emission Characteristics and Testing of Control Concepts in an Activated Sludge Wastewater Treatment Plant with Alternating Aerobic and Anoxic Phases. Environ. Sci. Technol. 2019, 53, 21, 12485–12494. https://doi.org/10.1021/acs.est.9b04889

Crisnaningtyas, F dan Hanny V. (2016). Pengolahan limbah cair industri farmasi formulasi dengan metode anaerob-aerob dan anaerob-koagulasi. Jurnal Riset Teknologi Pencegahan Pencemaran Industri, 7 (1) : 13-22

D'Antoni, B.M., F. Iracà, M. Romero. (2017). Brief review on filamentous and bulking in activated sludge treatments : causes and mitigation. Technical Report. DOI: 10.13140/RG.2.2.29506.58560. available at: https://www.researchgate.net/publication/317433584

Doma, Hala S., Hala M. El-Kamah and Ahmed Salem. (2014). Treatment of Catering Wastewater Using a Combination of Up-Flow Anaerobic Sludge Blanket Followed by Down Flow Hanging Sponge Reactor. Life Science Journal 11(12s). http://www.lifesciencesite.com.

Du, X., Junlu Wang, Veeriah Jegatheesan and Guohua Shi. (2018). Dissolved oxygen control in activated sludge process using a neutral network-based adaptive PID algorithm. Appl. Sci. 2018, 8, 261; doi:10.3390/app8020261

Ebie, Y., Towprayoon, S., Chiemchaisri, C., Mander, Ü., & Nogueira, S. F. (2013). Constructed Wetlands for Wastewater Treatment. Wetlands Supplement, 24. http://doi.org/10.3390/w2030530

Geovana, P. G., Dinara, G. A., Marcos, F. J., Alexandre, L.N., Camila, F. de P., Leonardo, D. B. da S., & Antônio, C. F. de M. (2016). Removal of nitrogen and phosphorus from cattle farming wastewater

using constructed wetland system. African Journal of Agricultural Research, 11(44), 4542–4550. https://doi.org/10.5897/AJAR2016.11425

Handayani, NI., Rustiana Yuliasni, Nanik Indah Setianingsih, Agung Budiarto. (2020). Full Scale Application of Integrated Upflow Anaerobic Filter (UAF)-Constructed Wetland (CWs) in Small Scale Batik Industry Wastewater Treatment. Jurnal Riset Teknologi Pencegahan Pencemaran Industri, 11 (1), 27-35

Henze, M., Mark CM van Loosdrecht, George A Ekama, Damir Brdjanovic. (2008). Biological Wastewater Treatment: Principles, Modeling and Design. IWA Publisher. ISBN: 9781843391883. DOI: 10.2166/9781780408613

Himanshu, B. (2011). Bacterial degradation of Azo Dyes and its derivatives. Thesis PhD, Saurashtra University

IPCC – Intergovernmental Panel on Climate Change. (2006). IPCC Guidelines for National Greenhouse Gas Inventories. Prepared by the National Greenhouse Gas Inventories Programme, Egglestone H.S., Buenfia L., Miwa K., Ngara T. and Tanabe K. (eds). Published: IGES, Japan.

KLH – Kementrian Lingkungan Hidup. (2012). Pedoman Penyelenggaraan Inventarisasi Gas Rumah Kaca Nasional Buku I Pedoman Umum

Kozak, M., Cirik, K., & Başak, S. (2021). Treatment of textile wastewater using combined anaerobic moving bed biofilm reactor and powdered activated carbon-aerobic membrane reactor. Journal of Environmental Chemical Engineering,9(4),105596.https://doi.org/https://doi.org/10.1016/j.jece.2021.105596

Lettinga, G., & Hulshoff Pol, L. (1991). UASB-Process design for various types of wastewater. Water Science and Technology, 24(8), 87–107.

Marlena, B., Rustiana Y., Sartamtomo, Agung Budiarto, Syarifa Arum, Misbachul Moenir, Cholid Syahroni. (2018). Removal of ammonia on catfish processing wastewater using horizontal sub-surface

flow constructed wetland (HSSFCW). Jurnal Riset Teknologi Pencegahan Pencemaran Industri, 9 (1), 15-21

Marlena, B., Syahroni, C., Sartamtomo, S., Zen, Nur. (2016) Pengolahan limbah organik dengan upflow anaerobic sludge blanket di industri kecap. Jurnal Riset Teknologi Pencegahan Pencemaran Industri, 7 (2), 81-87

Martins, A.M.P., Krishna Pagilla, Joseph J. Heijnen, MarkC.M. van Loosdrecht. (2004). Filamentous bulking sludge—a critical review. Water Research 38 (2004)793817.https://www.oieau.org/eaudoc/system/files/documents/39/196194/196194_doc.pdf

Meer, R. R. Van Der, & Vletter, R. De. (2016). Anaerobic treatment of wastewater : the gas-liquid sludge separator, 54(11), 1482–1492.

Moenir, M., Sartamtomo, S., & Moertinah, S. (2014). Pengolahan air limbah industri teh botol dengan teknologi biologis anaerobik UASB–wetland. Jurnal Riset Teknologi Pencegahan Pencemaran Industri, 5(2), 59–66.

Mulas, M., Francesco C., Jukka S., Seppo H., Riku V., (2016). Full-scale implementation of an advanced control system on a biological wastewater treatment plant. IFAC-PapersOnLine Volume 49, Issue 7, Pages 1163-1168. https://doi.org/10.1016/j.ifacol.2016.07.360

Ng, K.K. et al., .(2014). A novel application of anaerobic bio-entrapped membrane reactor for the treatment of chemical synthesis-based pharmaceutical wastewater. Separation and Purification Technology, 132, pp. 634-643. Available at : http://dx.doi.org/10.1016/j.seppur.2014.06.021

Peraturan Daerah Provinsi Jawa Tengah No 5 Tahun 2012 Tentang Perubahan Atas Peraturan Daerah Provinsi Jawa Tengah Nomor 10 Tahun 2004 Tentang Baku Mutu Air Limbah

Peraturan Menteri Lingkungan Hidup No. 68 Tahun 2016 Tentang Baku Mutu Air Limbah Domestik

Permen LHK Nomor P.16/Menlhk/Setjen/Kum.1/4/2019 Tentang Perubahan Kedua Atas Peraturan Menteri Lingkungan Hidup Nomor 5 Tahun 2014

Primasari, B., Shaliza Ibrahim, M Suffian M Annuar and Lim Xung Ian Remmie. (2011). Aerobic Treatment of Oily Wastewater: Effect of Aeration and Sludge Concentration to Pollutant Reduction and PHB Accumulation. Proceeding World Academy of Science, Engineering and Technology, Volume 5 No. 6. ISSN 2010-376X. Available at : https://www.researchgate.net/publication/283070 550_

Purwanta W dan Susanto JP. (2009). Emisi GRK Sektor Sampah dan Limbah Cair Perkotaan di Indonesia. JTekling hal 41-47

Ranieri, E., Silvia Giuliano, Ada Cristina Ranieri. (2021). Energy consumption in anaerobic and aerobic based wastewater treatment plants in Italy. Water Practice and Technology 16 (3): 851–863. https://doi.org/10.2166/wpt.2021.045

Seghezzo, L. (2004). Anaerobic treatment of domestic wastewater in subtropical regions. Thesis Wageningen University, Wageningen, the Netherlands – with references with summaries in English, Dutch, and Spanish. ISBN: 90-8504-029-9. https://www.researchgate.net/publication/347363 97

Setianingsih, N. I., Harsono, D., Zen, N., Crisnaningtyas, F., & Handayani, N. I. (2020). Implementasi Instalasi Pengolahan Air Limbah Biologi Terintegrasi Untuk Mengolah Air Limbah Campuran Domestik Dan Produksi. In Seminar Nasional Teknologi Industri Hijau (Vol. 2, No. 1, pp. 159-168).

Setianingsih, N.I., Sartamtomo, Harsono, D. (2021). Desain Instalasi Pengolahan Air Limbah Domestik Dengan Sistem Biologi Anaerob-Wetland. In Seminar Nasional Sains and Entrepreneurship (Vol. 1, No. 1, SNSE : VII).

http://conference.upgris.ac.id/index.php/snse/artic le/view/2100

Tan, K.N. (2019). A Detergent Destruction Method Used for Aerobic Treatment of Wastewater High in Detergent Content (WHD). International Journal of Environmental Science and Development 10(8):236-240 DOI:10.18178/ijesd.2019.10.8.1179

Tianzhi, W., Weijie, W., Hongying, H., & Khu, S.-T. (2021). Effect of coagulation on bio-treatment of textile wastewater: Quantitative evaluation and application. Journal of Cleaner Production, 312, 127798. https://doi.org/https://doi.org/10.1016/j.jclepro.2 021.127798

Vistanty H, Aris M, Novarina IH. (2015). Pengolahan Air Limbah Industri Karton Box dengan Metode Integrasi Upflow Anaerobic Sludge Bed (UASB) Reactor dan Elektrokoagulasi-Flotasi. Jurnal Riset Teknologi Pencegahan Pencemaran Industri. Vol. 6, No.1.DOI: http://dx.doi.org/10.21771/jrtppi.2015.v6.no1.p1 %20-%208

Wei, Y., Renze T. Van Houten , Arjan R. Borger, Dick H. Eikelboom, Yaobo Fan. (2003). Minimization of excess sludge production for biological wastewater treatment. Water Research 37(18):4453-67. DOI:10.1016/S0043-1354(03)00441-X

Yuliasni, R., N.I. Setyaningsih, N.I. Handayani, A. Budiarto. (2017) The performance of combined technology Upflow anaerobic reactor (UAR)-activated sludge (AS) for treating batik wastewater, Adv. Sci. Lett. 23. https://doi.org/10.1166/asl.2017.8725.

The Effect of Bentonite and Palm Shell Ash on The Mechanical and Physical Properties of Geopolymer Concrete

Muhammad Amin*[1], Yugo Chambioso[2], Suharto[1], Roniyus Marjunus[2], Yusup Hendronursito[1]

[1]National Research and Innovation Agency

[2]Physics Department, Faculty of Mathematics and Natural Science - Universitas Lampung

ARTICLE INFO	ABSTRACT
	Geopolymer concrete is an alternative to obtaining environmentally friendly mortar by synthesizing materials that contain a lot of aluminum silicate. This study aims to determine the effect of bentonite and palm shell ash composition on geopolymers' physical and mechanical characteristics. All materials are mashed, mixed, and molded with a 5x5x5 cm^3 cube. Ten specimens were prepared with bentonite - palm shell ash compositions are 40/45, 45/40, 50/35, 55/30, and 60/25 wt%. Meanwhile, the composition of NaOH, Na_2SiO_3, superplasticizer and water remained at 1.3, 7.7, 2, and 5 wt%, respectively. Then the samples were dried at room temperature for 24 hrs and heated at 60 °C or 80 °C for 12 hrs. The geopolymer concrete with the best characteristics was obtained with a composition of 40 wt% bentonites and 45 wt% palm shell ash by heating at 80 °C. This specimen has a compressive strength of 11.94 MPa with a density of 2.42 g/cm^3, porosity of 8.43%, and absorption of 3.48%. The results have a chemical composition of 55.59% SiO_2, 9.45% Al_2O_3, and 8.22 Fe_2O_3 with a dominant quartz phase. Scanning electron microscope photo shows good bonding between particles, and there are no pores formed.

1. INTRODUCTION

Ordinary Portland cement-based mortar is now the most used building material in the world. The annual use of cement reaches 4 billion tons with an annual growth rate of 4% (Mineral Commodities Summary, 2014). However, Portland cement production requires much energy and produces CO_2 gas that pollutes the environment (Pavithra, 2016). Generally, for every tonne of Portland cement production, one tonne of CO_2 is released into the atmosphere (Davidovits, 1994). Under these conditions, geopolymer concrete is one of the best options to reduce global warming. It can minimize CO_2 emissions by up to 80% (Pavithra, 2016).

Geopolymers are the latest innovation in concrete manufacturing worldwide. The conventional Portland cement is completely replaced with an aluminosilicate material activated by a strongly alkaline solution as a binder. (Patankar et al., 2013). Metakaolin, fly ash, red mud, agricultural waste, and mine waste are natural and industrial products used to make geopolymer binders (Slaty et al., 2013). Silica-rich materials such as fly ash, slag, rice husks, and aluminum-rich materials such as clays, including kaolin and bentonite, are significant parts of polymerization development (Part et al., 2015).

Palm shell ash is a pozzolanic material which is not bound like cement but contains dominant SiO_2 (Graille et al., 1985). Palm shell ash is obtained from a steam power

plant that uses palm kernel shells as fuel at temperatures from 800 - 1,000°C (Tangchirapat, 2009). Palm shell ash includes a large amount of silica dioxide and can be used as an alternative to cement. Palm shell ash is one of the pozzolanic materials found in most of the world. Palm shell ash can be used effectively to reduce cement use and waste volume, which is suitable for preserving the environment (Tangchirapat, 2009).

Some researchers used palm shell ash for an experiment. Production of geopolymer concrete using a mixture of fly ash and palm ash was well done by Islami et al. (2012). The highest compressive strength value occurs at the ratio of fly ash and palm ash 75:25, which is 20 MPa heated at a temperature of 110 °C. A higher compressive strength of geopolymer concrete can produce by mixed of ash from agro-industrial waste. The 25 MPa compressive strength was achieved from the 70:30 composition of fly ash and palm ash (Ariffin et al., 2017). Another experiment resulted from 44.57 MPa of geopolymer concrete compressive strength. This higher geopolymer compressive strength is produced from blast furnace slag and palm ash with a ratio of 0.2 (Yusuf, 2014).

Based on the previous studies, this research was conducted to see the effect of bentonite and palm shell ash on geopolymer cement's mechanical and physical properties.

2. METHODS

The parameters used for the design of the experiment are shown in Table 1. Palm shell ash is obtained from the fuel combustion process in a palm oil factory. Bentonite and palm shell ash were sieved on 100 mesh. Admixture of superplasticizer SP 200, NaOH (Merck), Na_2SiO_3 (Rofa, 58%), and water were added to the slurry according to the composition in Table 1. All materials are mixed and molded at 5x5x5 cm^3 cubes. The specimens are allowed to stand for 24 hrs and then heated in the oven at 60 °C and 80 °C for 12 hrs.

The geopolymer concrete was characterized by compressive strength, density, porosity, and absorption test. The compressive strength test was carried used the universal testing machine model HT-2402. The chemical content was analyzed by X-ray fluorescence using Malvern Panalytical Epsilon 3 and crystal phase by x-ray diffraction using Panalytical X'Pert 3 Powder. The topography of geopolymer was obtained by SEM Phenom Pro X.

3. RESULT AND DISCUSSION

XRF characterization was carried out to determine the chemical content used to manufacture geopolymer mortar. Bentonite with high Al_2O_3 content helps form bonds between concrete particles. While the dominant palm shell ash is silica, which is 51.47%. The chemical content of bentonite and palm shell ash overall can be shown in Table 2.

Based on Table 3 shows that the sample was heated at 80 °C and 60 °C, dominated by SiO_2, Al_2O_3, and Fe_2O_3 compounds. The results of the characterization of these samples follow XRF analysis of bentonite and palm shell ash raw materials, where the results of the analysis are dominated by SiO_2, Al_2O_3, and Fe_2O_3 compounds.

Table 1. Composition of geopolymer cement manufacture

Specimen	Bentonite (%)	Palm shell ash (%)	NaOH (%)	Na_2SiO_3 (%)	Superplasticizer (%)	Water (%)
I	40	45	1.3	7.7	2	5
II	45	40	1.3	7.7	2	5
III	50	35	1.3	7.7	2	5
IV	55	30	1.3	7.7	2	5
V	60	25	1.3	7.7	2	5

Table 2. Chemical composition of raw material

Compound	Bentonite (%)	Palm shell ash (%)
SiO_2	65.20	51.47
Al_2O_3	18.10	2.00
Fe_2O_3	9.41	4.50
K_2O	0.99	15.17
TiO_2	0.33	0.39
CaO	2.79	18.36
P_2O_5	0.12	5.09
NiO	0.09	-
SO_3	0.15	-
MnO	2.94	0.37
MgO	-	2.26

Table 3. Chemical composition of geopolymer

Compound	Composition (%, wt)	
	80 ℃	60 ℃
SiO_2	55.59	58.54
Fe_2O_3	8.22	9.43
Al_2O_3	9.45	11.73
CaO	13.10	9.74
$K2O$	7.74	5.51
TiO_2	0.53	0.51
MnO	0.44	0.30
P_2O_5	2.90	2.43
MgO	1.42	1.18

Based on Figure 1, the density values decreased due to increasing the ratio value. It has happened at temperatures of 60 °C and °80 C. The confidence level of the trend formed on this graph is 98% for temperatures 60 °C and 96% for 90 °C. The polymerization process is similar when heated at 60 °C to 90 °C. The temperature is close to perfect, and fast polymerization process (Duxson et al., 2007). However, the higher the temperature, the higher the evaporation process. A temperature of 80 °C causes a higher shrinkage of water content than a temperature of 60 °C, so the density is slightly different between these two temperatures. The density value is related to the porosity value. The higher the density, the smaller of concrete porosity. It creates higher compressive strength of the mortar (Malau, 2014).

Based on Figure 2, the porosity value is directly proportional to the ratio of bentonite ash. The confidence level of the trend formed on this graph is 95% for temperatures 60 °C and 91% for °80 C. The porosity value was closely related to the density value. This is because when the water in the geopolymer mortar evaporates, the pores that were previously filled with water become empty, and when the heating temperature is higher, the geopolymer mortar will dry out and form a tight bond and close the empty hole, causing the mortar to become denser. Therefore, the increased curing temperature used in geopolymer mortar will decrease the porosity value (Amin & Suharto, 2017).

Based on Figure 3, the absorption value is directly proportional to the temperature. The confidence level of the trend formed on this graph is 98% for temperatures 60 °C and 95% for 80 °C. The large pores in the geopolymer mortar, the more cavities are made. The empty cavity can absorb much water. High temperature caused less water to absorb in the geopolymer concrete (Amin & Suharto, 2017). In addition, the higher the heating temperature, the less the geopolymer mortar will absorb water. In other words, the smaller the absorption (Amin & Suharto, 2017). The low absorption value makes a low water absorption rate in the mortar. It is made higher the density value and compressive strength, and the mortar structure is getting tighter.

Based on Figure 4, the compressive strength value is directly proportional to temperatures. The density value obtained was high because the resulting mortar structure is dense. In addition, the compressive strength value is related to the porosity value and absorption value. If the compressive strength value is high, the porosity and absorption value will be smaller. The water granules in the geopolymer mortar will evaporate due to the use of high heating temperatures. Water evaporation is formed in smaller porosity in the mortar and increases the compressive strength value of the mortar.
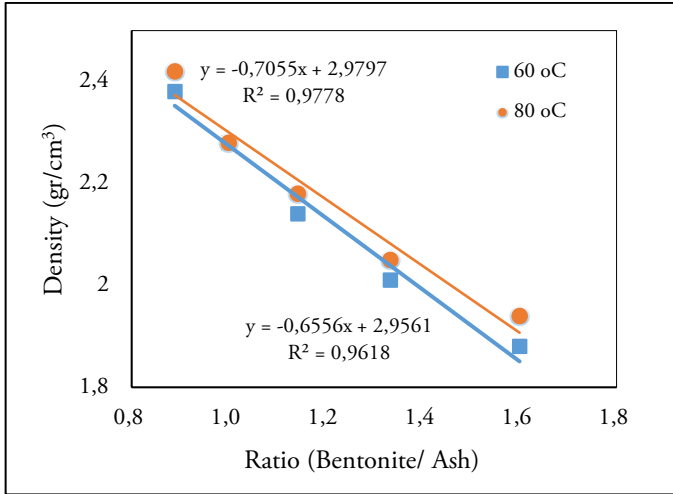
Figure 1. The graph of density vs ratio
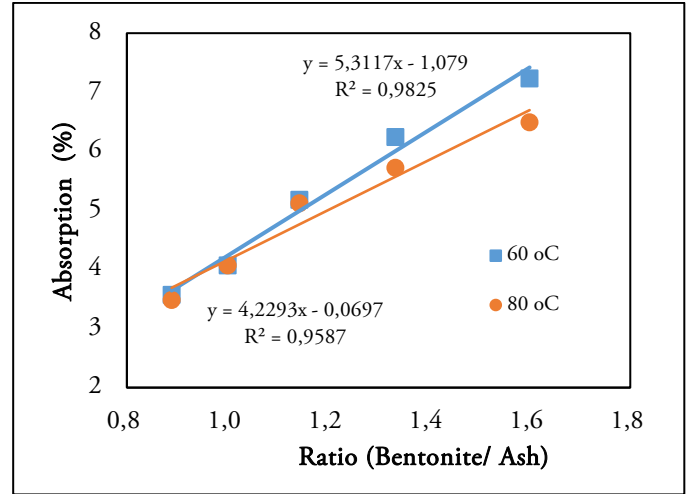
Figure 3. The graphic of absorption vs ratio
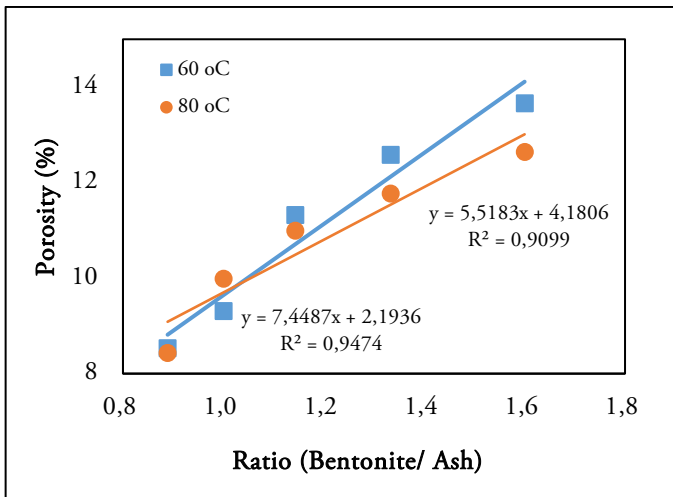
Figure 2. The graphic of porosity (P) vs ratio
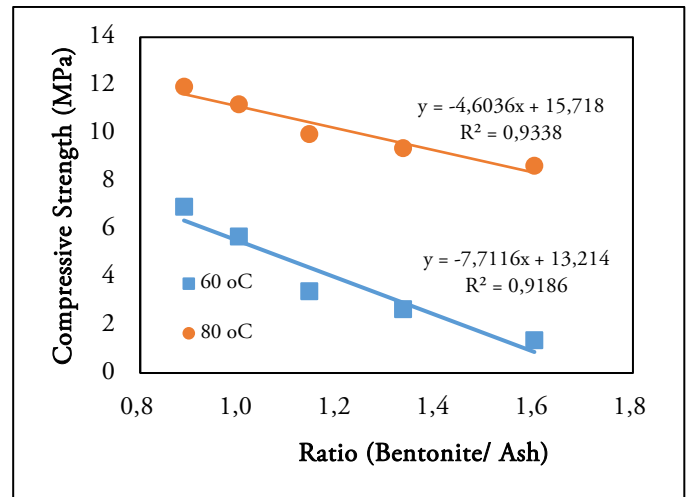
Figure 4. The graphic of compressive strength vs ratio

Geopolymer concrete made using geopolymer will bind with high alkaline NaOH to form a polysilicon-aluminate gel. It will harden due to the crystallization process and will increase the compressive strength of the mortar (Amin & Suharto, 2017). The increase in the percentage of bentonite causes a decrease in the compressive strength value due to an increase in porosity and changes in the microstructure. The addition of bentonite to the geopolymer increases the number of pores and pore size and widens the pore size distribution because bentonite contains much water (Yang et al., 2020).

XRD characterization was performed on samples with the highest compressive strength value (80 °C). The results of the X-Ray Diffraction test show that the higher the intensity, the higher the crystallinity level (Latif et al., 2014). The crystal phases formed are quartz. The crystal structure is hexagonal and is the highest peak on the chart, with its highest intensity at $2\theta = 26.654°$, as evidenced by the ICDD result 01-085-0795. Subsequently formed a sillimanite phase (Al_2SiO_4) with an orthorhombic crystal structure, its highest intensity at $2\theta = 27.584°$. The sillimanite phase showed conformity with the ICDD reference 01-089-0888. In the anorthite phase ($Ca(Al_2Si_2O_8)$) with the anorthic crystalline structure, its highest intensity at $2\theta = 31.310°$, the anorthite phase shows conformity with the ICDD reference 01-089-1460. In addition to the quartz, sillimanite and anorthite phases are formed, namely magnetite (Fe_3O_4) with an orthorhombic

crystal structure, the highest intensity of which is at the position of $2\theta=$ 19.791° with ICDD reference 01-076-0958. The intermediate microcline phase ($KAlSi_3O_8$) at position $2\theta=$ 36.646° with an anorthic crystalline structure.

The dominant phase formed is a quartz mineral group with the chemical formula silicon oxide (SiO_2), which indicates that the mortar has a lot of SiO_2, so it acts as a filler that fills the pores of the mortar and causes the mortar to have the highest compressive strength. The results are under the sample XRF test, where the compound produced is dominated by SiO_2.

X-ray diffraction analysis for two specimens has higher and lower compressive strength values. From the results of the XRD diffractogram obtained from the XRD analysis carried out in the study, the analysis is qualitative research, where the low peak does not indicate the number of crystals contained in the sample (Jefry, 2019). XRD analysis of specimen one at a temperature of 80 °C is shown in Figure 5.
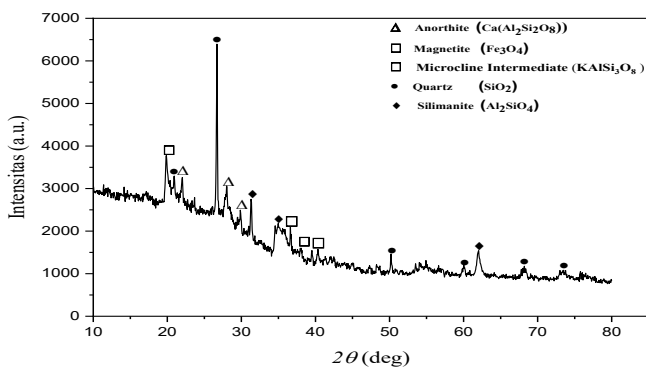
Figure 5. X-ray diffraction of temperature at 80 °C
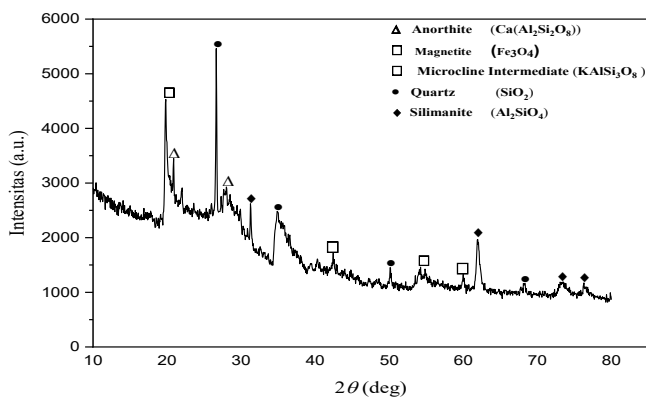
Figure 6. X-ray diffraction of temperature at 60 °C

XRD characterization was carried out on samples with the lowest compressive strength value (composition V at 60 °C). The results of the X-Ray Diffraction test show that the higher intensity, the higher the crystallinity level (Latif et al., 2014). The crystal phases formed are quartz. The crystal structure is hexagonal and is the highest peak on the chart, with its highest intensity at $2\theta=$ 26,644°, as evidenced by the ICDD result 01-085-0504. Subsequently formed a sillimanite phase (Al_2SiO_4) with an orthorhombic crystal structure, its highest intensity at $2\theta=$ 27,584°. The sillimanite phase showed conformity with the ICDD reference 01-089-0888. The anorthite phase ($Ca(Al_2Si_2O_8)$) with the anorthic crystalline structure, its highest intensity at $2\theta=$ 27,836°, the anorthite phase shows conformity with the ICDD reference 01-089-1461. In addition to the quartz, sillimanite and anorthite phases are formed, namely magnetite (Fe_3O_4) with an orthorhombic crystal structure, the highest intensity of which is at the position of $2\theta=$ 19,791° with ICDD reference 01-076-0958. And the intermediate microcline phase ($KAlSi_3O_8$) at position $2\theta=$ 42,423° with an anorthic crystalline structure.

The dominant phase formed is a quartz mineral group with the chemical formula silicon oxide (SiO_2). The results are under the sample XRF test, where the compound produced is dominated by SiO_2.

The results of the XRD diffractogram obtained from the XRD analysis have been carried out in the study. The analysis is qualitative research, where the low peak does not indicate the number of crystals in the sample (Jefry, 2019). XRD analysis of specimen 5 at 80 °C is shown in Figure 6.

Figure 7 depicts the morphology of the particle size SEM with a magnification of 2000X. The surface does not produce many pores (Jiminez et al., 2004). The distribution of constituent elements has a distribution of dominant elements in the form of Si, Al, and Fe.

The results of the EDS analysis are shown in Figure 8 where in the spectrum 0-2 KeV contains elements of carbon (C), oxygen (O), potassium (P), potassium (K), magnesium (Mg), aluminum (Al) and silicon (Si). In the energy spectrum of 2-4 KeV, there are elements of

potassium (K) and calcium (Ca), and in the energy spectrum of 4-7 KeV, there are elements of iron (Fe).
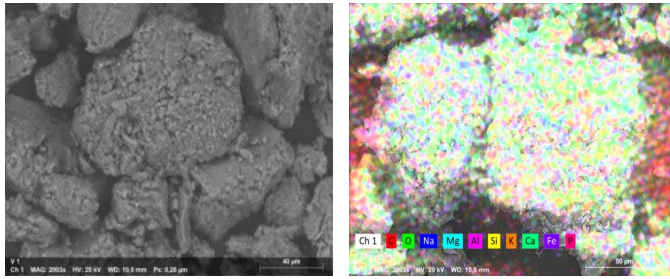
Figure 7. Micro photo of SEM for specimen 1 (temperature 80 °C)
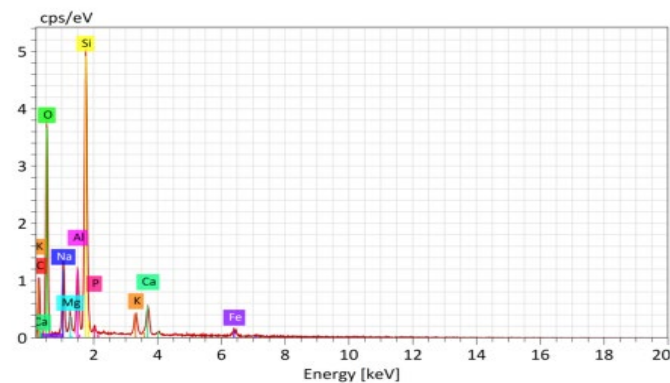
Figure 8. The result of EDS for specimen 1 (the temperature at 80 °C)

4. CONCLUSION

The high palm shell ash content and higher temperature increase the geopolymer compressive strength. This higher strength only used small content of bentonite. The best value obtained of 11.94 MPa with a density of 2.42 g/cm^3, porosity of 8.43%, and absorption of 3.48%. The chemical contained 55.59% SiO_2, 9.45% Al_2O_3, and 8.22% Fe_2O_3, with the phases formed in the form of quartz, sillimanite, anorthite, magnetite, and microcline intermediate. SEM results show that the surface does not produce many pores, so it has the highest compressive strength value. The lowest compressive strength value was obtained from the specimen with low content of palm shell ash. The low compressive strength was 6.94 MPa, with porosity and absorption value were 13.66% and 7.23%, respectively. The chemical contains 58.54% SiO_2, 11.73% Al_2O_3, and 9.43 Fe_2O_3, with the phases formed not different from the high compressive strength specimen. The SEM results show that the surface has many pores, so it has the lowest compressive strength value. This research shows that bentonite and palm shell ash waste is feasible and can be used in geopolymer cement manufacture.

REFERENCES

Amin, M., & User, S. 2017. Pembuatan semen geopolimer ramah lingkungan berbahan baku mineral basal guna menuju lampung sejahtera. Inovasi Pembangunan: Jurnal Kelitbangan, 5(01), 30-45.

ASTM C20-00. 2015. "Standard Test Methods for Apparent Porosity, Water Absorption, Apparent Specific Gravity, and Bulk Density of Burned Refractory Brick and Shapes by Boiling Water." ASTM International. https://doi.org/10.1520/C0020-00R10.2.

Davidovits, J. 1994. Global warming impact on the cement and aggregates industries. World resource review, 6(2), 263-278.

Duxson, P., Fernández-Jiménez, A., Provis, J. L., Lukey, G. C., Palomo, A., dan van Deventer, J. S. 2007. Geopolymer technology: the current state of the art. Journal of materials science, 42(9), 2917-2933.

Graille, J., Lozano, P., Pioch, D., dan Geneste, P. 1985. Essais d'alcoolyse d'huiles végétales avec des catalyseurs naturels pour la production de carburants diesels.

Islami, A. N., Saputra, E., dan Olivia, M. 2015. Kajian Parameter Mortar Geopolimer Menggunakan Campuran Abu Terbang (Fly Ash) dan Abu Sawit (Palm Oil Fuel Ash). In Prosiding 2nd Andalas Civil Engineering National Conference 160-167.

Jiminez, A. M. F., Lachowski, E. E., Palomo, A., & Macphee, D. E. 2004. Microstructural characterization of alkali-activated PFA matrices for

waste immobilization. Cement and Concrete Composites, 26(8), 1001-1006.

Malau, F. B. 2014. Penelitian Kuat Tekan dan Berat Jenis Mortar Untuk Dinding Panel dengan Membandingkan Penggunaan Pasir Bengkulu dan Pasir Baturaja dengan Tambahan Foaming Agent dan Silica Fume. Jurnal Teknik Sipil dan Lingkungan. Jurusan Teknik Sipil Universitas Sriwijaya. 2 (2).

Mineral Commodity Summaries. 2014. US Department of the Interior US GeologicalSurvey.http://minerals.usgs.gov/mineral s/pubs/mcs/2014/mcs2014/ (accessed 10. 03.21).

Mohd Ariffin, M. A., Hussin, M. W., dan Rafique Bhutta, M. A. 2011. Mix design and compressive strength of geopolymer concrete containing blended ash from agro-industrial wastes. In Advanced Materials Research (Vol. 339, 452-457). Trans Tech Publications Ltd.

Part, W. K., Ramli, M., dan Cheah, C. B. 2015. An overview on the influence of various factors on the properties of geopolymer concrete derived from industrial by-products. Construction and Building Materials, 77, 370-395.

Patankar, S. V., Jamkar, S. S., dan Ghugal, Y. M. 2013. Effect of water-to-geopolymer binder ratio on the production of fly ash based geopolymer concrete. Int. J. Adv. Technol. Civ. Eng, 2(1), 79-83.

Pavithra, P. E., Reddy, M. S., Dinakar, P., Rao, B. H., Satpathy, B. K., dan Mohanty, A. N. 2016. A mix design procedure for geopolymer concrete with fly ash. Journal of cleaner production, 133, 117-125.

Slaty, F., Khoury, H., Wastiels, J., dan Rahier, H. 2013. Characterization of alkali activated kaolinitic clay. Applied Clay Science, 75, 120-125.

Tangchirapat, W., Jaturapitakkul, C., dan Chindaprasirt, P. 2009. Use of palm oil fuel ash as a supplementary cementitious material for producing high-strength concrete. Construction and Building Materials, 23(7), 2641-2646.

Yang, Y., Jiang, J., Hou, L., Lu, Z., Li, J., & Wang, J. 2020. Pore structure and properties of porous geopolymer based on pre-swelled bentonite. Construction and Building Materials, 254, 119226.

Yusuf, M. O., Johari, M. A. M., Ahmad, Z. A., dan Maslehuddin, M. 2014. Strength and microstructure of alkali-activated binary blended binder containing palm oil fuel ash and ground blast-furnace slag. Construction and Building Materials, 52, 504-510.

The Kinetic Analysis and Adsorption Isotherm of Chicken Egg Shells and Membranes Against Synthetic Dyes

Linda Hevira*[1], Gampito[2]

[1]University of Mohammad Natsir, Bukittinggi, Indonesia
[2]Islamic University of Mahmud Yunus, Batusangkar, Indonesia

ARTICLE INFO	ABSTRACT
	Textile industry waste at this time is enough to worry the community and the environment. The presence of synthetic dyes in water is hazardous, even in small concentrations. These synthetic dyes are derivatives of aromatic compounds such as benzene, toluene, and naphthalene, which are more resistant and stable than natural dyes. The adsorption method is used because it is easier to do, has no side effects, and does not require complicated and expensive equipment. In this study, the shells and membranes of discarded chicken eggs became useful as an absorbent of indigo carmine dye with an adsorption capacity of 6.399 mg/g. The adsorption reaction kinetics were analyzed from the optimal contact time data, and the reaction isotherm was analyzed from the adsorption optimal concentration data. The kinetic model that fits the research is the second pseudo-order with R^2 = 0.9998. The adsorption mechanism demonstrates that the adsorption capacity is proportional to the adsorbent's active sites. The adsorption isotherm model, with R^2 = 0.9748, is more closely related to the Freundlich isotherm model, indicating that adsorption occurs in several layers. From an economic point of view, chicken egg shells and membranes can be recommended as dye absorbers that are eco-friendly, efficient, and simple to obtain while lowering organic solid waste.

1. INTRODUCTION

Along with the rapid population and industry growth, the volume of waste released into the environment is increasingly unstoppable. One of these wastes is textile waste in synthetic dyes that damage human health and the environment. For example, synthetic dyes can disrupt the ecosystem of aquatic biota, even in small concentrations. This is due to reduced sunlight, which can interfere with aquatic plants' photosynthesis and cause acute toxicity to aquatic life (Sharma, Dalai, & Vyas, 2017). Meanwhile, waste discharged into nature without being processed first will pollute the surrounding environment. For example, if wastewater is discharged to the ground, it will make the soil

become damaged and reduce fertility. In addition, industrial waste can pollute the river because of the many chemicals contained in it. Eye irritation, skin irritation, mutagenicity, and carcinogenicity are all side effects of these colours (Hevira and Zein, 2022; Wang et al., 2017)

Many methods for treating dyed wastewater have been reported, including chemical coagulation, activated sludge, biodegradation and magnetic separation (Rahmayeni, Arief, Jamarun, Emriadi, & Stiadi, 2017), and nanofiltration (Abid, Zablouk, & Abid-Alameer, 2012). However, this method is still not widely used because of the high cost and long process. Currently, the government is promoting and supporting the use of waste by providing other benefits to adsorb waste using green technology

(Hevira, Ariza, & Rahmi, 2021). Meanwhile, from an economic perspective, the use of eggshells can reduce the cost of processing textile waste and also has the potential to be developed in Indonesia.

One of the appropriate methods is the adsorption method. The adsorption method is the most commonly used because it is reliable, has no harmful side effects, and does not necessitate complicated and expensive equipment. Biosorption is an adsorption method that utilizes natural adsorbents (Hevira, Zein, & Ramadhani, 2019) derived from plants such as orange peel (Arami, Limaee, Mahmoodi, & Tabrizi, 2005), melon peel (Djelloul & Hamdaoui, 2015), and banana peel (Abudi, Lattieff, Chyad, & Abbas, 2018). In addition, temporary animal waste can be utilized, such as chitosan from fish scales (Iqbal et al., 2011), crab shells (Fatombi et al., 2019), and chicken feathers (Bagaskoro et al., 2020).

Chicken egg shells are often not utilized and even become waste in large quantities, which are sent to landfills with high management costs. Whereas chicken egg shells contain mostly calcium carbonate and have 10,000-20,000 pores, they can be used as an adsorbent. Chicken egg shells can be utilized as a calcium supplement and green manure. The skin's membrane can also be used as cosmetics because they contain collagen (Faridi & Arabhosseini, 2018). Meanwhile, egg white has been used as a modifier to adsorb dyes (Rahmiana Zein et al., 2022). The ability of chicken eggshells to adsorb pollutants is because it has many pores and functional groups such as C-H, C-C, C-O, C=O, NH, and SH that can bind with cations or anionic compounds (Hevira, Rahmi, et al. 2020). The use of chicken egg shells is a low-cost adsorbent (Carvalho, Araujo, & Castro, 2011) that can absorb dyes in the textile industry. Besides, the eggshell membrane has amino acids that can interact with dyes.

Previous research showed that the use of egg shells and their membranes has a good adsorption capacity (Pramanpol & Nitayapat, 2006) (Hevira, Rahmi, et al., 2020). Therefore, this time the author will look at the reaction kinetics tested using the first pseudo-order, second pseudo-order, and equations of intra-particle diffusion.

Meanwhile, the Langmuir and Freundlich isotherm equations are used to perform adsorption analysis.

2. METHODS

2.1. Adsorbent Preparation

Chicken egg shells and membranes (CESM) were collected in Bukittinggi, West Sumatra, Indonesia. Nitric acid, NaOH, indigo carmine dye, and aquadest. Instruments: shaker, pH meter, spectrophotometer UV-Vis. Procedures: CESM washed with flowing water, dried, and in a blender using (Turbo 8099). After that, it was sieved with a particle size of 36 μm (Hevira, Rahmi, et al. 2020). Then 0.1 g of CESM with a particle size of 36 μm was added to 50 mL dye solution with variation concentration, then stirred with a shaker at 100 rpm with the respective optimum contact time. After that, the solution was filtered, and the filtrate was analyzed by UV-vis spectrophotometer at max.

2.2. Activation of an Adsorbent

In 75 millilitres of 0.01 N HNO$_3$, 25 grams of CESM was immersed for 2 hours to open the pores of CESM and activate the active adsorbent (Sopiah, Prasetyo, and Aviantara 2017). After that, the CESM was rinsed with distilled water until the pH returned to normal. After drying, CESM was ready for use.

2.3. Determination of Optimal Contact Time for Adsorption

At the optimum pH previously determined, 0.1 g CESM is added to 25 mL indigo carmine at a concentration of 10 mg/L into erlenmeyer 50 mL. The addition of nitric acid and base is used to change the ph level. The stirring time ranged between 15 and 60 minutes at 100 rotations per minute. The adsorption process was then filtered, and the concentration was determined using a UV–Vis spectrophotometer.

Adsorption capacity against indigo carmine calculated by equation 1:

$$q_e = \frac{(C_o - C_e)V}{m} \qquad (1)$$

Where Co and Ce denote the initial and equilibrium dye concentrations (mg/L), m denotes the mass of CESM (g), and V denotes the volume of the indigo carmine reaction mixture (L).

2.4. Reaction Kinetics

Reaction kinetics analysis predicts the speed at which adsorbate is transferred from solution to adsorbent. In this research, the reaction kinetics can be seen from the reaction kinetics of the indigo carmine in CESM. The first pseudo-order (Lagergren) and second pseudo-order adsorption kinetics models were used to calculate the adsorption kinetics equations (Ho & Mc Kay).

$$-\ln(q_e - q_t) = k_1 t - \ln q_e \tag{2}$$

$$\frac{t}{q_t} = \frac{1}{k_2 q_e^2} + \frac{1}{q_e} \tag{3}$$

Where :

q_e = equilibrium adsorption capacity in mg / g

q_t = time t adsorption capacity in mg/g

k_1 denotes the first pseudo-order reaction rate constant in minutes -1

k_2 denotes the second pseudo-order rate constant in g/mg.min

The intra-particle diffusion model was used to explain the adsorption process. As shown in equation 4, the Weber and Morris equations express intra-particle diffusion.

$$q_t = K_{ip} t^{0.5} + C \tag{4}$$

Where K_{ip} (µmol/ g. min$^{0.5}$) is the constant rate intra-particle diffusion, and C (µmol/g) is the thickness layer limit, with plotting qt versus t$^{0.5}$ then we get the slope and intersection of straight lines in the form of K_{ip} and C (Marcel et al. 2019).

2.5. Determination of the Initial Dye Concentration

The same procedure used to evaluate the time available was used to determine the early concentration of indigo carmine. The dye studied, in this case, has an initial concentration of 10-50 mg/L.

2.6. Isotherm of Adsorption

The isotherm of adsorption is determined by the relationship between the concentration of the adsorbed solute on the solid and the concentration of the solution. Langmuir isotherm is used to determine whether adsorption occurs in the monolayer or not, while the isotherm Freundlich assumed that adsorption occurs in a multilayer manner. The formula used in this case is the Langmuir and Freundlich equation.

$$\frac{1}{q_e} = \frac{1}{q_m k_L} \frac{1}{C_e} + \frac{1}{q_m} \tag{5}$$

$$k_L = \frac{1}{q_m a} \tag{6}$$

$$R_L = \frac{1}{1 + (1 + k_L C_e)} \tag{7}$$

$$\log q_e = \log k_F + \frac{1}{n} \log C_e \tag{7}$$

Where :

q_m : capacity adsorption maximum

q_e : capacity adsorption in state balanced

C_e : ion concentration in state balanced

k_L : Langmuir's constant Among sorbent with sorbate

R_L is the separation factor, where R_L in the form of bad ($R_L > 1$), linear ($R_L = 1$), beneficial ($0 < R_L < 1$), and irrecoverable ($R_L = 0$).

k_F : Constant of Freundlich denoting capacity adsorption

$1/n$: Intensity adsorption

3. RESULT AND DISCUSSION

3.1. The Influence of Agitation Time

The Influence of agitation time greatly affects whether or not adsorption occurs. In Figure 1, we can see that as the agitation time of the reaction between the indigo carmine and CESM increases, the adsorption capacity decreases. Although the reduction is minimal, the capacity adsorption of The optimum CESM against indigo carmine occurred at a 15 minutes contact time. This fast time is possible because indigo carmine is an anionic dye that will quickly interact with eggshell membranes which contain lots of amino acids. The same thing also happened during the adsorption of indigo carmine using Ketapang shells; the adsorption capacity was low initially (Hevira, Zilfa, et al. 2020). Then if it is modified with egg white which contains

rich amino acids, the adsorption capacity will increase (Rahmiana Zein et al., 2022). This is also the advantage of this research compared with Rahmiana Zein's studies. This research is better because it is more effective and efficient in terms of time and cost, besides it is also easy to implement, as explained in part 3.5. However, there are still shortcomings; the amount of $CaCO_3$ contained in eggshells can affect the hardness of water (Aidha, 2013).

Meanwhile, suppose the contact time between the adsorbate and the adsorbent continues to be increased after reaching the optimum capacity. In that case, it will potentially inhibit the adsorption of the adsorbate and even release the bonds between the adsorbate and the adsorbent so that the adsorption capacity will decrease.
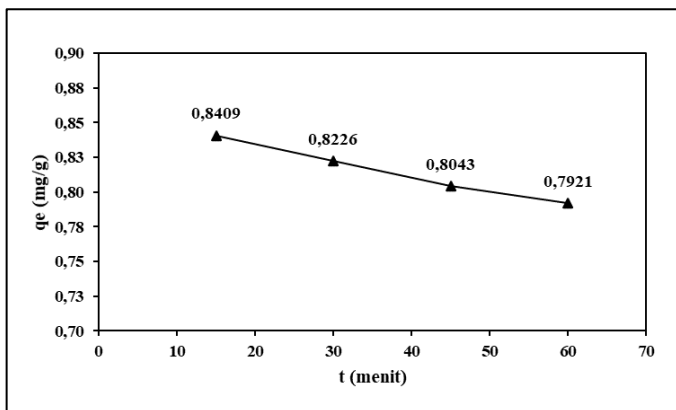
Figure 1. Effect of contact time on adsorption capacity of CESM to adsorb indigo carmine

3.2. Reaction Kinetics

The first pseudo-order model was derived from the Lagergren reaction rate equation for liquid and solid adsorption based on solid capacity. While the second pseudo-order is suggested that the number of available sites on the adsorbent determines the adsorption ability. (Liu et al. 2016).

Figures 2A and 2B show that the R^2 value of the first-order pseudo equation is 0. 9912, while the coefficient of determination of the second pseudo-order is 0.9998. Thus the second pseudo-order kinetic model is a better way to explain the reaction rate for indigo carmine in CESM (Budnyak et al. 2018).

Figure 2C shows that the adsorption process in the intra-particle diffusion equation begins with the passage of particles from outside the adsorbent to the adsorbent's surface, followed by the diffusion of molecules into the pores. (Holle, Wuntu, and Sangi 2013). For dye adsorption by CESM, the coefficient of determination (R^2) is 0.9972, which means that the only model that restricts the adsorption rate is the intra-particle diffusion model.

Table 1. CESM's Kinetic Parameter of IC Adsorption

Variant Parametric	Variant Parametric	CESM +IC
Trial Data	$q_{e\,(exp)}$ (mg/g)	0.8409
First pseudo-order	k_1 (min^{-1})	0.0007
	$q_{e\,(calc)}$ (mg.g^{-1})	1.6043
	R^2	0.9912
Second pseudo-order	$k2$ (g mg^{-1} minute^{-1})	0.9215
	$q_{e\,(calc)}$ (mg.g^{-1})	0.7763
	R^2	0.9998
Intra- particle diffusion	C	0.8910
	K_{diff} (mg.g^{-1} min$^{-0.5}$)	0.0128
	R^2	0.9972

Table 1 shows that the value of q_e in the treatment and q_e in the pseudo-second-order equation are closer, namely 0.8409 with 0.7763. This slightly adjacent value is confirmed by an R^2 value of 0.9998. Meanwhile, the value of q_e obtained in the experiment and qe in the pseudo-first-order equation is further, namely 0.8409 and 1.6043. This value is confirmed by the value of R^2, which is 0.9912. The same result also happened to the adsorption of indigo carmine by *Ocimum gratissimum* (Adewumi O. Dada et al. 2020).

Figure 2. Adsorption kinetics of indigo carmine dye utilizing (A) first pseudo-order kinetics, (B) second pseudo-order kinetics, (C) intra-particle diffusion model

3.3. The Influences of the Early Dye Concentration

The influences of the early dye concentration were investigated in the 10 to 50 mg/L range. The adsorption capacity of CESM against indigo carmine increases as the 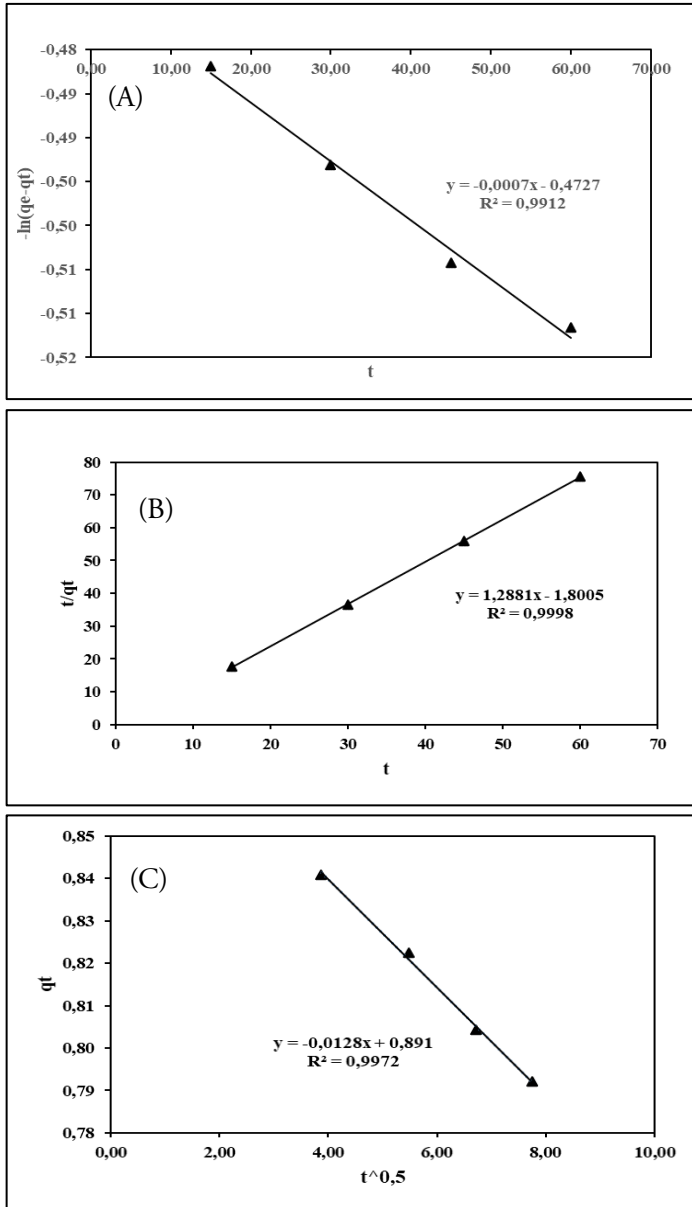concentration of the dye indigo carmine increases. With increasing concentrations of both dyes, the amount adsorbed at equilibrium increases. This is because enhancing the initial dye level enhances the diffusion's primary driver, i.e., concentration gradient, which favours the velocity at which dyes migrate from solutions to the surface of the adsorbent (Marcel et al. 2019). At a concentration of 50 mg/L, Figure 3 demonstrates that CESM had an optimal adsorption capacity against indigo carmine of 6.3963 mg/g. The adsorption capacity is quite high compared to fluoride adsorption on eggshells (Bhaumik et al. 2012).

Meanwhile, the greater the starting concentration of indigo carmine, the more active side of the adsorbate or CESM will be saturated so that the adsorption capacity will decrease (Hevira and Zein, 2022).

3.4. Adsorption Isotherm

Isotherm Adsorption is a connection among many components absorbed by the adsorbent when the state is in equilibrium at a constant temperature. Isotherm adsorption is a function of concentration substance solute that is adsorbed on the solid to concentration solution.

In Figure 4, it can be seen that the coefficient of determination of the Langmuir equation used is 0.9474. While the value of the coefficient of determination using the Freundlich isotherm is 0.9748. Since the value is closer to 1, this data indicates that the Freundlich equilibrium model is more appropriate for the data gathered from the experiment. It demonstrated that indigo carmine could be absorbed using CESM more dominant in multilayer. The isotherm of Freundlich assumes the surface of the adsorbent was heterogeneous, and each molecule has potency different adsorption. The same thing also happened to the adsorption of metal ions using the Ketapan shell (Hevira, Munaf, and Zein, 2015). The value of the adsorption intensity or n from the Freundlich isotherm model is 0.6424. It suggests that the intensity has increased of adsorption of the dye with the biosorbent went well because it was in the range of 1-10.

In the meantime, the correlation coefficient value of the Langmuir model is 0.9474, as shown in Table 2. Its worth is also quite good, indicating that the adsorption also occurs in a monolayer. This is confirmed by the RL value of 0.5631, where if the RL is greater than 0 and smaller than 1 at equilibrium, it indicates that the adsorption is going well (A. O. Dada, Ojediran, and Olalekan 2013).
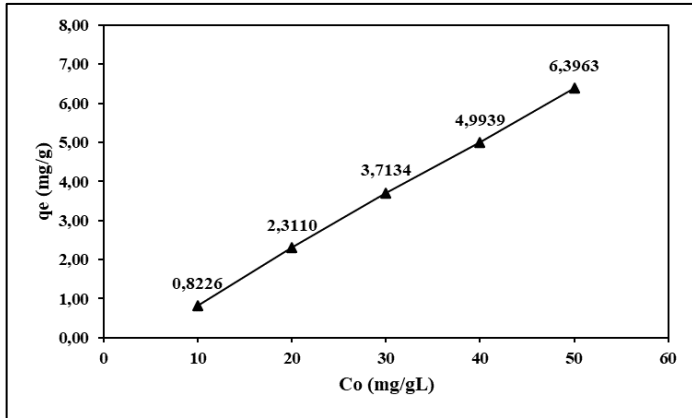
Figure 3. The effect of early dye concentration at the start on CESM's ability to eliminate indigo carmine
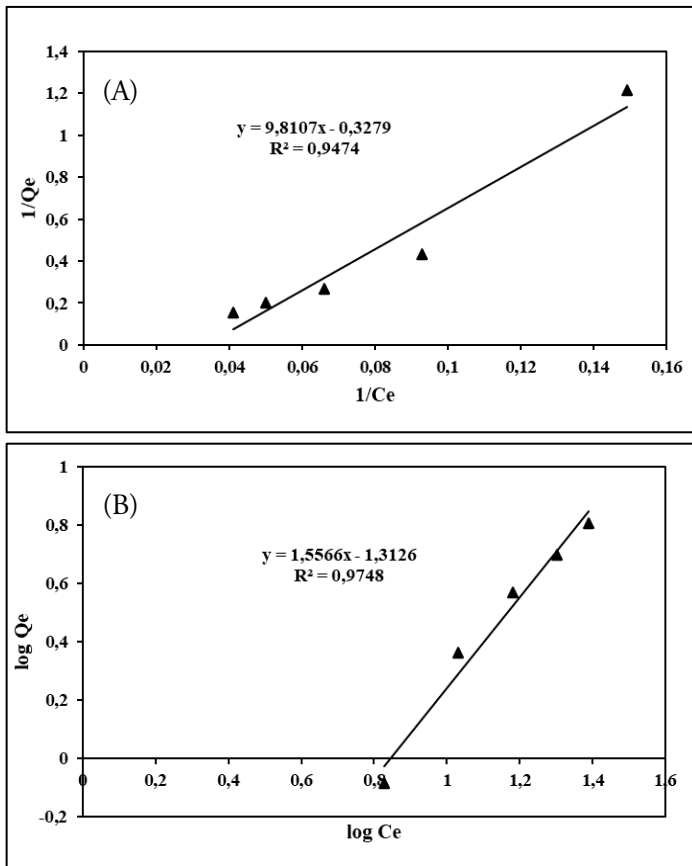
Figure 4. (A) Langmuir, (B) Freundlich isotherm linear equation of indigo carmine dye adsorption at CESM

3.5. Analysis of Adsorption Costs

A cost analysis of the colour waste treatment was also conducted from an economic viewpoint. In many studies, adsorbents used as activated carbon generally have a high absorption capacity, such as chitosan-activated carbon (Fatombi et al. 2019) and date palm-derived activated carbon (Khadhri et al. 2019). However, if the adsorbent is activated with acid, the absorption capacity is almost the same as that of the activated carbon adsorbent. This was also proven by Gupta et al. when negatively absorbing charged Cr(VI) metal ions, similar to the absorption of indigo anionic dyes. The absorption cost of 1 g Cr(VI) using acid-modified bagasse is 11 times cheaper than the absorption of Cr(VI) using bagasse-activated carbon with almost the same adsorption capacity (Gupta, Gupta, and Kharat 2018). A similar result also proves that eggshells have a better adsorption capacity than activated carbon (Misfadhila et al., 2018).

Table 3 shows the estimated cost for treating adsorbents before contact with dyestuffs, excluding using reagents and other definite means with the same treatment to adsorb indigo carmine dye. We can see that adsorption using egg shells at an IC concentration of 50 ppm is very cheap. However, when compared with the adsorption of iC using egg white with crosslinker N, N′-Methylenebis (acrylamide) can adsorb anionic dyes (indigo carmine) with an adsorption capacity at an IC concentration of 50 ppm is 26.25 mg g-1 (Oymak & Esra Bağda, 2018). Although the adsorption capacity value is quite high, the use of acrylamide is still dangerous and the costs used are high.

Table 2. Isotherm Model for IC adsorption by CESM

Isotherm	Parameter	CESM+IC
Langmuir	k_L (L /mg)	0.0334
	q_m (mg/g)	3.0497
	ALL	0.5631
	R^2	0.9474
Freundlich	k_F	0.0487
	N	0.6424
	R^2	0.9748

Table 3. Comparison of The Cost of Processing Adsorbent with Other Adsorbents

No.	Material (100 g)	price (SGD) in sigmaaldrich.com	price (IDR) raw material and processing services	adsorption capacity (mg/g) in 50 ppm dye solution	reference
1	1 kg activated carbon peanut shell	-	10,000 (estimation)	20.11	(Fatombi et al. 2019)
2	1 kg dried eggwhite as crosslinker		20,000	12.35	(Rahmiana Zein et al. 2022)
3	1 kg ketapang shell	-	10,000	5.46	(Hevira, Zilfa, et al. 2020)
4	1 kg g N,N'- methylenebis (acrylamide) as crosslinker	97,40	103,244 (10 % usage estimate)	26.25	(Oymak and Esra Bağda 2018)
5	1 kg eggshell and its membrane	-	2000	6.3963	This study

4. CONCLUSION

From the research data analysis, it can be concluded that CESM (chicken eggshell and membrane) can adsorb indigo carmine dye. The absorption mechanism shows that the kinetic model is more suitable with the second pseudo model, where the adsorption capacity is proportional to the number of active sites of the adsorbent. Meanwhile, intra-particle diffusion was revealed to be the only one that limits the adsorption rate. The adsorption capacity of CESM was 6,3963 mg/g, while the adsorption isotherm follows the Freundlich isotherm model. It means that the adsorption takes place in a multilayer manner. From an economic point of view, CESM has the potential to be recommended as a dye adsorber in reducing textile industry waste because the cost is low, easy, and fast.

REFERENCES

Abid, Mohammad Fadhil, Mumtaz Abdulahad Zablouk, and Abeer Muhssen Abid-Alameer. 2012. "Experimental Study of Dye Removal from Industrial Wastewater by Membrane Technologies of Reverse Osmosis and Nanofiltration." *Iranian Journal of Environmental Health Science and Engineering* 9(17): 1.

Abudi, Zaidun Naji, Farkad Ali Lattieff, Tasnim Fahem Chyad, and Mohammed Nsaif Abbas. 2018. "Isotherm and Kinetic Study of the Adsorption of Different Dyes from Aqueous Solution Using Banana Peel by Two Different Methods." 7(2): 220–29.

Aidha, Novi Nur. 2013. "Aktivasi Zeolit Secara Fisika Dan Kimia Untuk Menurunkan Kadar Kesadahan (Ca Dan Mg) Dalam Air Tanah (Activation of Zeolite by Physical and Chemical Methods To Reduce The Hardness (Ca and Mg) OF GROUNDWATER) Novi Nur Aidha." *J. Kimia Kemasan* 35(1): 58–64.

Arami, Mokhtar, Nargess Yousefi Limaee, Niyaz Mohammad Mahmoodi, and Nooshin Salman Tabrizi. 2005. "Removal of Dyes from Colored Textile Wastewater by Orange Peel Adsorbent: Equilibrium and Kinetic Studies." *Journal of Colloid and Interface Science* 288(2): 371–76.

Bagaskoro, Arief Panji et al. 2020. "Adsorben Logam Fe dalam Air Tanah." 01(01): 1–8.

Bhaumik, R. et al. 2012. "Eggshell Powder as an Adsorbent for Removal of Fluoride from Aqueous Solution: Equilibrium, Kinetic and Thermodynamic Studies." *E-Journal of Chemistry* 9(3): 1457–80.

Budnyak, Tetyana M. et al. 2018. "Methylene Blue Dye Sorption by Hybrid Materials from Technical Lignins." *Journal of Environmental Chemical Engineering* 6(4): 4997–5007.

Carvalho, J., J. Araujo, and F. Castro. 2011. "Alternative Low-Cost Adsorbent for Water and Wastewater Decontamination Derived from Eggshell Waste: An Overview." *Waste and Biomass Valorization* 2(2): 157–67.

Dada, A. O., J. O. Ojediran, and Abiodun Paul Olalekan. 2013. "Sorption of Pb2+ from Aqueous Solution unto Modified Rice Husk: Isotherms Studies." *Advances in Physical Chemistry* 2013.

Dada, Adewumi O. et al. 2020. "Sustainable and Low-Cost Ocimum Gratissimum for Biosorption of Indigo Carmine Dye: Kinetics, Isotherm, and Thermodynamic Studies." *International Journal of Phytoremediation* 0(0): 1524–37.

Djelloul, Chawki, and Oualid Hamdaoui. 2015. "Dynamic Adsorption of Methylene Blue by Melon Peel in Fixed-Bed Columns." *Desalination and Water Treatment* 56(11): 2966–75.

Faridi, Hamideh, and Akbar Arabhosseini. 2018. "Application of Eggshell Wastes as Valuable and Utilizable Products: A Review." *Research in Agricultural Engineering* 64(2): 104–14.

Fatombi, Jacques K. et al. 2019. "Adsorption of Indigo Carmine from Aqueous Solution by Chitosan and Chitosan/Activated Carbon Composite: Kinetics, Isotherms and Thermodynamics Studies." *Fibres and Polymers* 20(9): 1820–32.

Gupta, Meenal, Harsh Gupta, and D S Kharat. 2018. "Environmental Technology & Innovation Adsorption of Cu (II) by Low-Cost Adsorbents and the Cost." *Environmental Technology & Innovation* 10: 91–101.

Hevira, Linda, Zilfa, et al. 2020. "Biosorption of Indigo Carmine from Aqueous Solution by Terminalia Catappa Shell." *Journal of Environmental Chemical Engineering* 8(5): 104290.

Hevira, Linda, Azimatur Rahmi, et al. 2020. "The Fast and Low-Cost-Adsorbent for the Removal of Cationic and Anionic Dyes Using Chicken Eggshell with Its Membrane." *Mediterranean Journal of Chemistry* 10(3): 294–301.

Hevira, Linda, Dinda Ariza, and Azimatur Rahmi. 2021. "Pembuatan Biofoam Berbahan Dasar Ampas Tebu Dan Whey." *Jurnal Kimia dan Kemasan* 43(2): 75–81.

Hevira, Linda, Edison Munaf, and Rahmiana Zein. 2015. "The Use of Terminalia Catappa L. Fruit Shell as Biosorbent for the Removal of Pb(II), Cd(II) and Cu(II) Ion in Liquid Waste." *Journal of Chemical and Pharmaceutical Research* 7(10): 79–89.

Hevira, Linda, and Rahmiana Zein. 2022. *Monograf: Komparasi Penyerapan Zat Warna Kationik Dan Anionik Pada Biosorben Cangkang Ketapang*. Andalas University Press.

Hevira, Linda, Rahmiana Zein, and Putri Ramadhani. 2019. "Review Metoda Adsorpsi Pada Penyerapan Ion Logam Dan Zat Warna Dalam Limbah Cair." *Jurnal Sains dan Terapan Kimia* 13(1): 39–58.

Holle, Rizky B., Audy D. Wuntu, and Meiske S. Sangi. 2013. "Kinetika Adsorpsi Gas Benzena Pada Karbon Aktif Tempurung Kelapa." *Jurnal MIPA* 2(2): 100.

Iqbal, Javed et al. 2011. "Adsorption of Acid Yellow Dye on Flakes of Chitosan Prepared from Fishery Wastes." *Arabian Journal of Chemistry* 4(4): 389–95.

Khadhri, Nisrine, Mohamed El Khames Saad, Mongi Ben Mosbah, and Younes Moussaoui. 2019. "Batch and Continuous Column Adsorption of Indigo Carmine onto Activated Carbon Derived from Date Palm Petiole." *Journal of Environmental Chemical Engineering* 7(1).

Liu, Jiayang et al. 2016. "Adsorption of Methylene Blue on an Agro-Waste Oiltea Shell with and without Fungal Treatment." *Nature Publishing Group* (November): 1–11.

Marcel, C et al. 2019. "Indigo Carmine and 2, 6-Dichlorophenolindophenol Removal Using Cetyltrimethylammonium Bromide-Modified Palm Oil Fiber : Adsorption Isotherms and Mass

Transfer Kinetics." *International Journal of Biomaterials* 2019.

Misfadhila, Sestry, Zikra Azizah, Cynthia Diane, and Putri Chaniago. 2018. "Pengaplikasian Cangkang Telur Dan Karbon Aktif Sebagai Adsorben Logam Timbal." 10(2): 1–8.

Oymak, Tulay, and Esra Bağda. 2018. "Crosslinked Egg White as Eco-Friendly, Reusable and Cost-Effective Biosorbent for Rapid Removal of Indigo Carmine." *Clean - Soil, Air, Water* 46(6): 1–18.

Pramanpol, Nuttawan, and Nuttakan Nitayapat. 2006. "Adsorption of Reactive Dye by Eggshell and Its Membrane." *Kasetsart Journal - Natural Science* 40(SUPPL.): 192–97.

Rahmayeni et al. 2017. "Magnetically Separable ZnO-MnFe2O4 Nanocomposites Synthesized in Organic-Free Media for Dye Degradation under Natural Sunlight." *Oriental Journal of Chemistry* 33(6): 2758–65.

Sharma, Komal, AK Dalai, and RK Vyas. 2017. "Removal of Synthetic Dyes from Multicomponent Industrial Wastewaters." *Reviews in Chemical Engineering* 34(1): 107–34.

Sopiah, Nida, Djoko Prasetyo, and Dwindrata B Aviantara. 2017. "Pengaruh Aktivasi Karbon Aktif Dari Tandan Kosong Kelapa Sawit Terhadap Adsorspi Kadmium Terlarut." *Jurnal Riset Teknologi Pencegahan dan Pencemaran Industri* 8(2): 55–66.

Wang, Wenxia et al. 2017. "Transport Behaviors of Anionic Azo Dyes at Interface between Surfactant-Modified Flax Shives and Aqueous Solution: Synchrotron Infrared and Adsorption Studies." *Applied Surface Science*.

Zein, R. et al. 2010. "Removal of Pb(II), Cd(II) and Co(II) from Aqueous Solution Using Garcinia Mangostana L. Fruit Shell." *Journal of Hazardous Materials* 181(1–3): 52–56.

Zein, Rahmiana et al. 2022. "The Improvement of Indigo Carmine Dye Adsorption by Terminalia Catappa Shell Modified with Broiler Egg White." *Biomass Conversion and Biorefinery* (0123456789).

Analysis of Potential Utilization of Sarulla Geothermal Combined Cycle Residual Fluids for Direct Use in The Coffee Industry

Jonius Christian Harefa*[1], Hadiyanto[2], Udi Harmoko[3]

[1]Master of Energy, Diponegoro University, Semarang, Indonesia

[2]Chemical Engineering, Diponegoro University, Semarang, Indonesia

[3]Department of of Physics, Diponegoro University, Semarang, Indonesia

ABSTRACT

The Geothermal Power Plant is one of the new renewable energy power plants. In Indonesia, the realization has reached 2%. Sarulla Operations Limited is the first geothermal power plant in Indonesia, located in North Tapanuli Regency, that utilizes combined cycle technology. Coffee is the leading commodity in the North Tapanuli district, with a plant area of 17,586 hectares. Coffee is dried in the traditional way (open field drying) so that it is still constrained by rain and cloudiness and can only be done during the day. The reinjection well fluid has a temperature of 103°C with a flow rate of 4978 t/h and a pressure of 6–14 Bar. This study analyses the residual fluid energy for coffee drying purposes. Energy and exergy calculations are done manually and using DWSIM software with a total of 24 data points 24 hours a day to represent the availability of dryers both day and night. The results showed that the most energy needed to raise the drying air temperature at night from 15°C to 60°C was 125.62 kW, while the lowest energy needed to raise the drying air temperature during the day from 30°C to 40°C was 27.92 kW. The results of research calculations show the energy potential for residual fluid from geothermal plants to be used for drying coffee for 24 hours, both day and night.

1. INTRODUCTION

The application of anaerobic digestion (AD) in GPP (Geothermal Power Plant) is one of the new renewable energy power plants. Geothermal energy is one of the new renewable energies developed in Indonesia to date (Rame, Purwanto, & Sudarno, 2021). Figure 1 shows that until Q3-2021, the realization of increasing geothermal power plant capacity reaches 2% of the total of 11.2% of Indonesia's new renewable energy mix. The new renewable energy mix in 2019 in Indonesia reached 9.15%, increasing from 2.05% to 11.2% in Q3-2021 (Nagel, Dwiatmoko, & Windarta, 2022). Therefore, energy in Indonesia must immediately transition from fossil fuels to new renewable energy aimed at conserving natural resources (Ariawan, Windarta, & Dwiatmoko, 2022). The geothermal energy potential in Indonesia is the second largest in the world, with a potential of 23.76 gigawatts (GW), and the comparison of the realization of power plants with the existing geothermal energy potential is still below 10% (around 8.9%) (Mudassir, 2021).

According to the National Energy Council, one of the policies for optimizing the development of geothermal resources is to recommend using binary power plant technology for the use of medium-temperature geothermal (Siswanto, 2020). In addition, this policy encourages PLTP (Geothermal Power Plant) to use a combined cycle to maximize the utilization of existing geothermal energy.
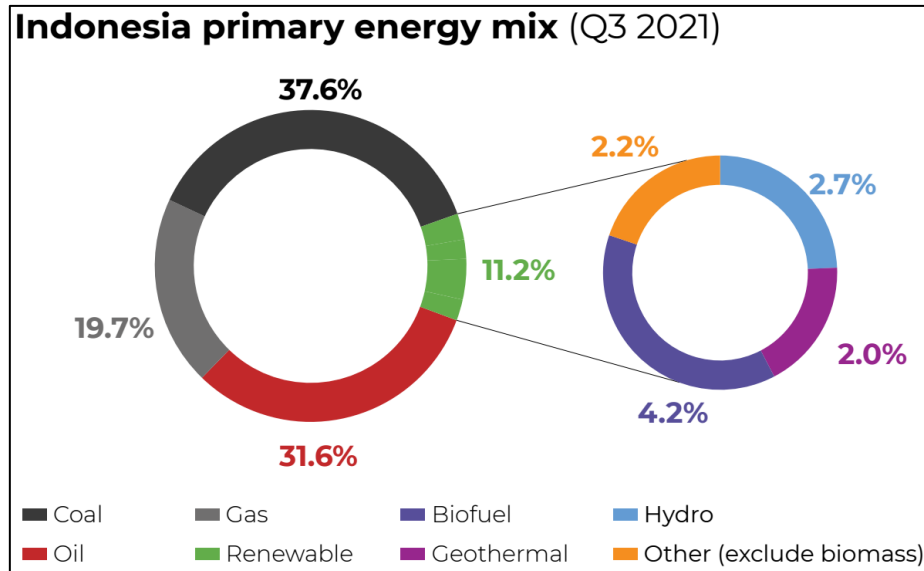
Figure 1. Indonesia Primary Energy Mix 2021 (IESR, 2021)
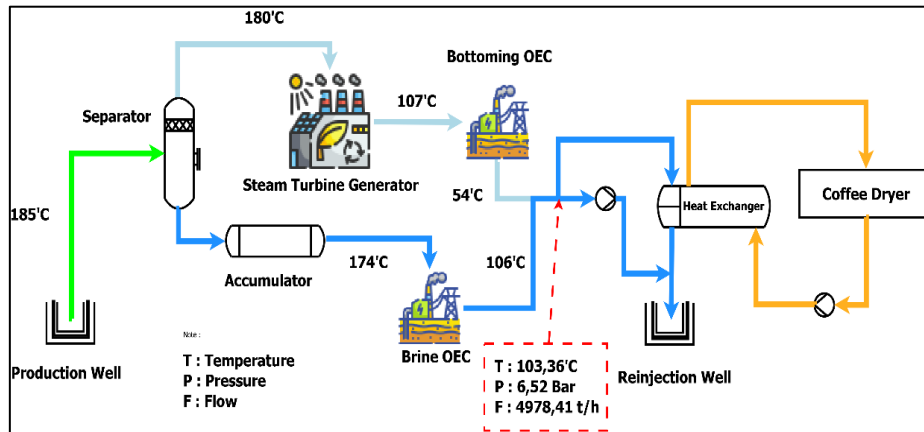
Figure 2. Research Concept Framework

Sarulla Geothermal Power Plant is a geothermal power plant located in North Tapanuli Regency, North Sumatra province. Sarulla is a consortium of several companies, including Medco Energi International Tbk., Itochu Corporation, Kyushu Electric Power Co., Inc., and Ormat (Wolf, 2015). Sarulla Operations Limited is Indonesia's first geothermal power plant that utilizes combined cycle technology. Ormat International developed this technology by combining single-flash technology with binary organic rankine cycle technology. The installed capacity of the generator is 330 MW (Rakhmadi & Sutiyono, 2015).

Geothermal fluids (geothermal production wells) produce steam (gas phase) and brine (liquid phase), which are then utilized indirectly by generating electricity, as shown in Figure 2. The steam rotates the turbine and produces 60 MW of energy at a pressure of around 10 bar and a temperature of about 180°C. The steam output from the turbine still has a temperature of 107°C, which flows to the Binary power plant Bottoming OEC (Ormat Energy Converter) through a heat exchanger and heats the second fluid, pentane, which has a low boiling point of around 30°C-400°C. The pentane, which has a low boiling point and has been heated, turns into a pressurized vapour, which is then used to turn a turbine and generate electricity with a total capacity of 7MW. The output steam from the generator is used towards the Bottoming OEC so that it is condensed into condensate at a temperature of around

54°C. The condensate at 54°C is directly injected back into the injection well into the earth after previously being combined with brine.

Brine (liquid phase) from production wells at a temperature of 174°C flows through a heat exchanger at Brine OEC. The principle used is almost the same as Bottoming OEC, namely heating pentane to turn it into a pressurized vapour and then turning a turbine and generating about 15MW of electricity. The brine output from the OEC Brine has a temperature of around 106°C. The remaining brine is combined with the condensate output from the Bottoming OEC and then injected back into the earth.

The residual fluid output from the generator in the form of condensate and brine, which has a temperature of around 103°C and is generally injected directly into the earth, can still be used for commercial business. According to (De Sousa & Domenici Roberto, 1998), the temperature of 90°C-95°C can still be maximized for community business development, as shown in Figure 3. Therefore, the authors want to maximize this potential for the development of further research.

In the early stages of its development, GPP Sarulla experienced resistance and obstacles from the local community. This was marked by the occurrence of rejection demonstrations in several locations requesting that the development of the Sarulla geothermal working area be stopped (Hutasoit, 2020). The community's refusal is based on the consideration that the existence of GPP will only disturb and damage the living environment and will not directly improve the local community's economy. Horizontal conflicts with local communities will always occur if the existence of GPP is not directly benefiting the community (Ahmad et al., 2021). The challenge of local community rejection can be reduced if the company is willing to empower local communities, especially in business development.
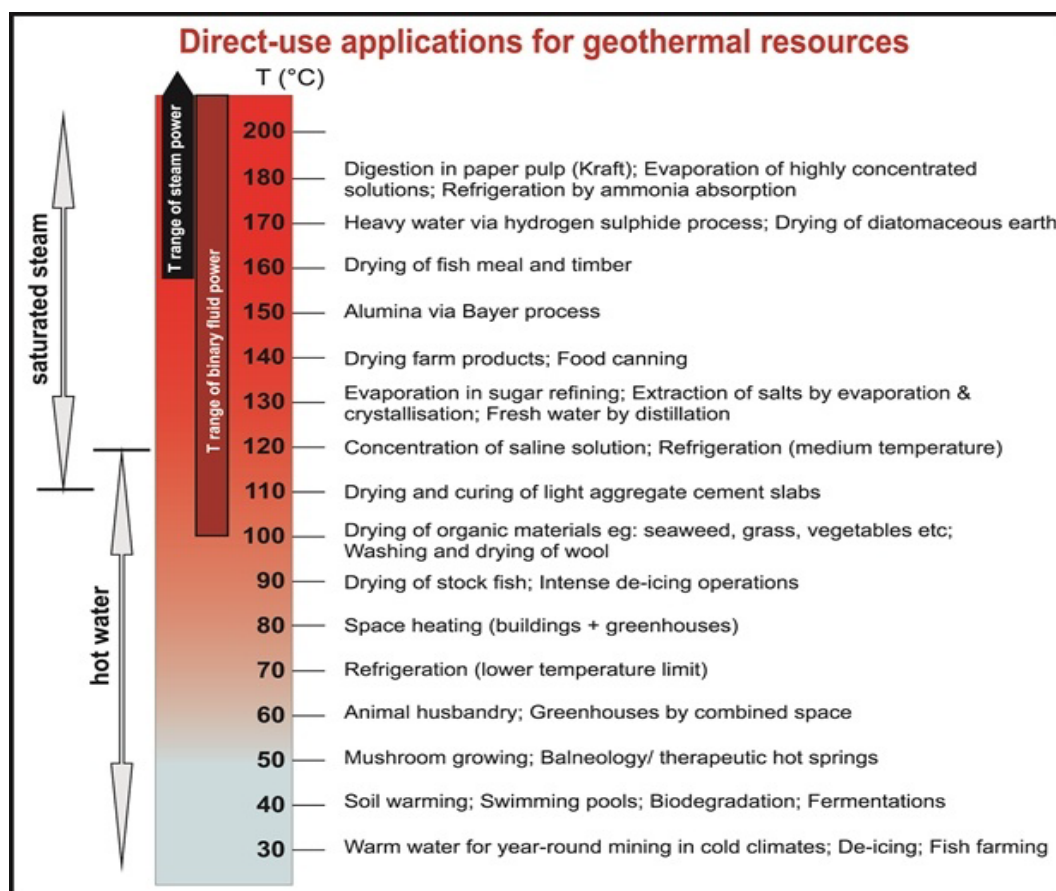

Figure 3. Lindal Diagram (Australian Academy of Science, 2015)
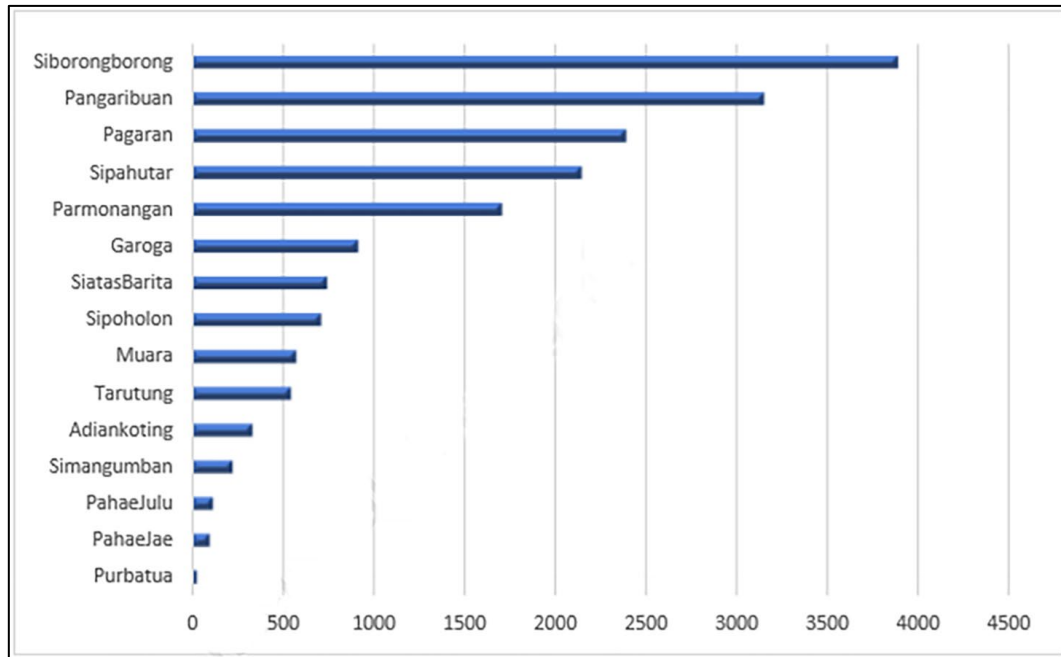
Figure 4. Coffee Production by Subdistrict in Tapanuli Utara Regency (ton) 2020 (BPS, 2021)

Figure 4 shows that coffee is the leading commodity in the North Tapanuli district. Including a coffee plant area coverage of 17,586 hectares, with the most significant plant area in the Siborongborong sub-district covering an area of 3,893.90 hectares (BPS, 2021).

This research is an answer to the local community's refusal to utilize the remaining geothermal fluid energy from the power plant in Sarulla to be used directly for drying coffee and direct use of geothermal energy in Mataloko to increase public acceptance (Ahmad et al., 2021). The fluid flowing into the reinjection well has a temperature of 103°C with a flow rate of 4978 t/h and a pressure of 6-14 bar. Therefore, the reinjected fluid energy can still be used directly for community business development in North Tapanuli, which is a coffee-producing area as a leading commodity (BPS, 2021), which still uses traditional coffee drying (drying in the open field) and is constrained by rain and cloudiness and can only be done during the day. This study analyzes the availability of energy and exergy for 24 hours a day so that coffee dryers can be carried out even though the weather is bad and at night.

2. METHODS

In this study, the authors used observational research methods (observation). As shown in Figure 5, this method collects data by recording the information during the study. The data processing method uses statistical testing means or the average value to get the average value for each variable with a total of 24 data points to describe the availability of the remaining fluid from the power plant for a full day for 24 hours. Secondary data from credible books and websites are needed to complete the research. Additional data comes from assumptions (like blower output in mass and pressure) to support calculations and simulations using DWSIM software. DWSIM is a chemical process simulation software that Daniel Wagner developed, and the software is open-source. The data is then processed to determine the energy and exergy values residual fluid can produce from the power plant.

Figure 5. Research Flowchart

3. RESULT AND DISCUSSION

3.1. Energy and Exergy

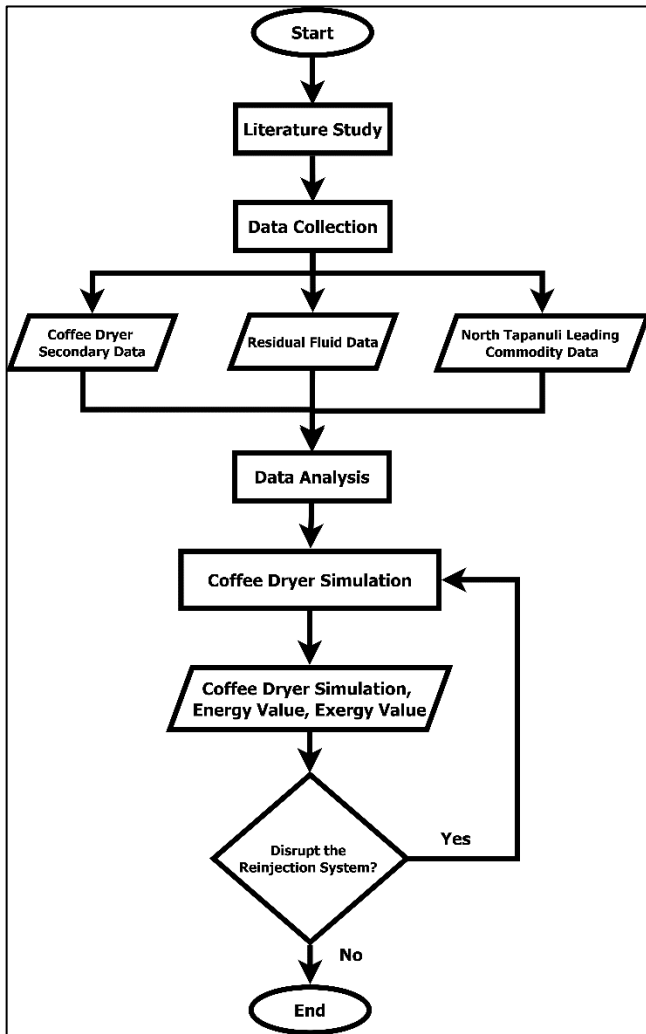Analysis of the performance of a system requires the concept of energy balance following the first law of thermodynamics. The first law of thermodynamics states that energy can neither be created nor destroyed. This law is often known as the law of conservation of energy. A system that changes from an initial state to a state of equilibrium or a final state can absorb and release energy into the system's surroundings. When no more changes exist in the system, a state of equilibrium is created. A state of equilibrium occurs when there is no change in the unbalanced force acting on it. The energy contained in the initial and final states makes it very difficult to determine the results of the total content, so measurements are carried out by measuring the difference between the energy of the initial state Jand energy in the final state and the energy exchanged between the system and its environment (Abdulaziz, 2020).

According to Rajput (Rajput, 2012), the energy balance that occurs in the heat exchanger can be determined with the assumption that no heat is lost to the environment and changes in potential and kinetic energy can be neglected. Then the equation for

$$Q_{hot} = m_h C_{ph}(T_h, in - T_h, out) \qquad (1)$$

$$Q_{cold} = m_c C_{pc}(T_c, out - T_h, in) \qquad (2)$$

The heat energy released by Qhot as a heat medium has the same value as the heat energy absorbed by Qcold as a heat conducting medium, so the equation is given.

$$Q = m_h C_{ph}(T_h, in - T_h, out) = m_c C_{pc}(T_c, out - T_c, in) \qquad (3)$$

Where m is the flow rate value in kg/s, and Cp is the specific heat value at constant pressure in J/kg. K, T is the fluid temperature in Kelvin or Celsius, while the symbols h and c refer to the hot fluid h (hot) and cold fluid c (cold). The heat transfer in the heat exchanger media varies throughout the heat exchanger area. This value can be determined by LMTD (logarithmic mean temperature difference). The LMTD for a heat exchanger with a counter-flow arrangement is determined by the equation:

$$\theta_m = \frac{\theta_1 - \theta_2}{\ln\left(\frac{\theta_1}{\theta_2}\right)} \qquad (4)$$

Where θ_m is the LMTD in °C units, θ_1 is the difference between $T_{c,in}$, which is the temperature of the hot fluid input and $T_{c,out}$, which is the temperature of the cold fluid output in °C units, θ_2 is the difference between $T_{c,out}$, which is the temperature of the hot fluid output, while $T_{c,in}$, is the temperature of the cold fluid entered in units of °C.

The LMTD value, according to Kreith (Kreith, Manglik, & Bohn, 2011), can be used to determine the overall heat transfer coefficient in the heat exchanger with the equation:

$$q = UA\overline{\Delta T} \qquad (5)$$

Where q is the heat energy in W units, and U is the overall heat transfer coefficient in the heat exchanger in units of $W/m2.K$, A is the heat transfer surface area in units of m², and $\overline{\Delta T}$ is the LMTD (θ_m). From equation 5, we get the following equation :

$$A = \frac{q}{(U)(\overline{\Delta T})} \qquad (6)$$

Equation 6 can determine the heat exchanger's total heat transfer surface area in m².

Calculation of exergy, according to (Moran, Shapiro, Boettner, & Bailey, 2014), is carried out by evaluating the change in the total exergy flow from the input flow to the output flow in the heat exchanger by ignoring kinetic energy and potential energy. The determination of the exergy change can be calculated using the following equation :

$$m(e_2 - e_1) = m(h_2 - h_1) + T_o(s_2 - s_1) \tag{7}$$

Where $m(e_2 - e_1)$ is the exergy of the hot fluid flow in units of W, $m(h_2 - h_1)$ is the difference between the enthalpy value of the hot fluid output and the enthalpy of the incoming hot fluid multiplied by m as mass, $T_o(s_2 - s_1)$ is the difference between the entropy of the hot fluid output and the entropy of the hot fluid entering it multiplied by T_o as the ambient reference temperature in °C. The symbol number 2 refers to the hot fluid output, and the number 1 refers to the hot fluid input. Equation 7 has the same principle in determining the exergy value for cold fluids using the equation :

$$m(e_4 - e_3) = m(h_4 - h_3) + T_o(s_4 - s_3) \tag{8}$$

Number 4 refers to the cold fluid output, and number 3 refers to the cold fluid input. The exergy destruction value in the heat exchanger can be determined by the equation:

$$E_d = m(e_2 - e_1) + m(e_4 - e_3) \tag{9}$$

Where E_d is the exergy destruction value in W units, while $m(e_2 - e_1)$ is the exergy of the hot fluid flow in W units, and $m(e_4 - e_3)$ is the exergy of the cold fluid flow in W units.

Figure 6 shows the reinjection brine data, taken from the brine output and condensate used to generate electricity, which flows to the reinjection well. Brine output from Brine OEC and condensate from vapour condensation at Bottoming OEC from 2 units, namely Unit 1 and Unit 2 of the Sarulla NIL Power Plant, are then combined and flowed to the reinjection well. Table 1 shows the data taken from pressure, temperature, and brine flow rate data. They were taken from the central control room of the power plant on October 31, 2021, when there were 9 production wells available out of a total of 11 production wells. Two production wells are under periodic inspection and maintenance.

Table 1. Brine Reinjection Data

Parameter	Temperature (°C)	Pressure (Barg)	Flow Rate (Kg/h)
Highest Value	106,360	6,83	5.009.644
Lowest Value	101,578	6,29	4.944.730
Average Value	103,360	6,52	4.978.410
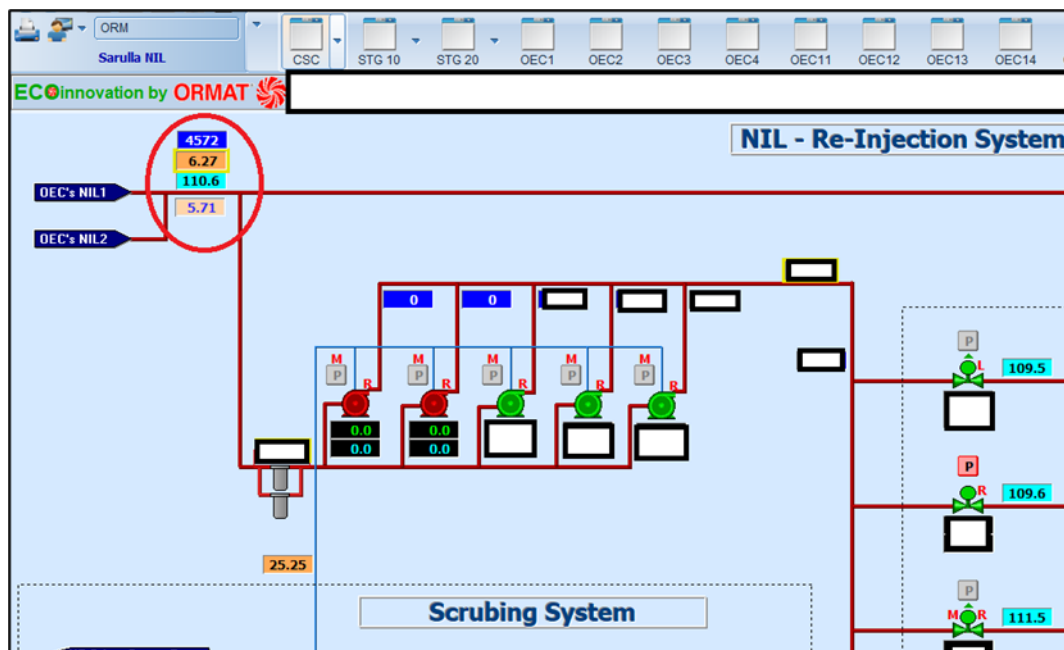
Figure 6. Research Data Collection Point

Table 2. Air Temperature Data as an Input

Data source	Range	Information
BMKG (BMKG, 2022)	Minimum : 13,0 °C – 16,5 °C	The temperature in the North Tapanuli area
	Maximum: No information	
Weatherspark (Weather Spark, 2022)	Minimum: 18°C – 19 °C	Sarulla's temperature
	Maximum: 27 °C – 29 °C	

Table 3. Data on Coffee Drying Temperature

Data source	Temperature
Balai Pengkajian Teknologi Pertanian (BPTP) Lampung (BPTP Lampung, 2018)	40°C - 60°C
Rancang Bangun dan Pengujian Alat Pengering Biji Kopi Tenaga Listrik Dengan Pemanfaatan Energi Surya (Gultom & T., 2019)	45°C – 50°C
Perancangan Mesin Pengering Biji Kopi Semi Otomatis Kapasitas 25 kg (Fauzi & Widiantoro, 2021)	50°C – 55°C
Dispersion Coefficient of Coffee Berries in Vibrated Bed Dryer (Finzer, Sfredo, Sousa, & Limaverde, 2007)	40°C – 50°C
Karakteristik Pengerringan Biji Kopi Berdasarkan Variasi Kecepatan Aliran Udara Pada Solar Dryer (Yani & Fajrin, 2013a)	50°C – 55°C

The input air data to increase temperature is taken from the ambient air around the power plant. Table 2 shows that the data comes from 2 references, BMKG and Weatherspark. The data is in the form of a minimum and maximum temperatures achieved in the power plant area. The maximum air temperature represents the hot air temperature during the day, while the minimum air temperature represents the cold air temperature at night.

Coffee drying is carried out at a specific temperature to maintain the quality of the coffee beans so that there is no damage to the coffee beans. Suitable drying air temperatures for Arabica and Robusta coffee beans were varied in multiples of 10°C to 40°C, 50°C, and 60°C. Table 3 shows the temperature required for drying coffee.

3.2. Result of Energy Calculation

The overall energy balance of the heat exchanger can be assumed to be that the heat exchanger is well insulated, and the heat energy loss to the surroundings is insignificant and can therefore be neglected. The energy balance can be expressed by equation 3, where m is the mass flow value in kg/s. C_p is the specific heat at constant pressure in J/kg.K. T is the average fluid temperature in K, both the inlet (in) and outlet (out) temperatures. The symbols h and c refer to hot and cold media as heat conductors.

Table 4 shows the brine data parameters from the power plant used as input brine in the heat exchanger. The pressure value (p), the flow rate value (m), and the temperature value (t) are the average values of the overall data. The flow rate value is converted into units of kg/s, while for the specific heat, it is converted into units of J/kg.K. The specific heat value refers to the temperature of 375 K = 101,85°C, representing the specific heat value of the brine temperature of 103,360°C.

Table 5 shows the input air data parameters. The assumption of an air mass of 10 t/h is converted into units of kg/s and an air pressure of 2 bar gauge to describe the blower used to provide air intake to the dryer. The specific heat value of air (Cp) refers to the specific heat value of air at a temperature of 300 K = 26,85°C to represent the ambient air temperature of 25°C. The output air temperature refers to the temperature required for drying coffee beans.

The output temperature of the brine determined the heat transfer value from brine to air, which is already known by equation 1. The calorific value obtained from the brine mass product, the specific brine heat, and the difference between the input brine temperature and the output brine temperature value produce a value of heat energy from brine. The heat transfer value between brine and air with a mass of 10 t/h to reach a temperature of 50°C from an initial temperature of 25°C is 69.792 J/s or 70 kW.

Table 6 above shows the value of the energy required to raise the ambient air temperature for each temperature variation from the initial temperature to the expected final temperature for a dryer using equation 3 and equation 1.

Table 4. Parameters of Brine Data

Parameter	Pressure (p)	Flow Rate (m)	Temperature (t)	Specific Heat (Cp)
Value	6,52	4.978.410	103,360	4,220
Units	Barg	Kg/h	Celcius	kJ/kg.K
Conversion		1.382,892		4.220
Conversion Unit		Kg/s		J/kg.K
Information	Brine as input	Brine as input	Brine as input	375 K = 101,85 °C
Source	Primary data	Primary data	Primary data	Secondary Data

Table 5. Air Data Parameters

Parameter	Pressure (p)	Flow Rate (m)	Temperature Input (Tin)	Temperature Output (Tout)	Specific Heat (Cp)
Value	2	10.000	25	50	1,005
Units	Barg	Kg/h	Celcius	Celcius	kJ/kg.K
Conversion		2,78			1.005
Conversion Unit		Kg/s			J/kg.K
Information	Air Input	Air Input	Air Input	Air Output	300 K = 26,85 °C
Source	Assumption	Assumption	Secondary Data	Secondary Data	Secondary Data

Figure 7 shows that a large amount of energy is needed to raise the temperature from 15°C to 60°C at 125,62 kW, while the smallest amount of energy is needed to raise the temperature from 30°C to 40°C at 27,92 kW. This shows that the ambient air temperature in Table 2 dramatically affects the energy required to raise the air temperature for the coffee dryer.

The relatively high daytime temperatures require little energy to raise the temperature for drying. However, at night, when the ambient air temperature tends to be relatively low, it takes much energy to raise the temperature for drying purposes.

According to Kreith (Kreith et al., 2011), the heat transfer distribution in the heat exchanger between the heat medium and the heat conducting medium generally is not constant but varies along the heat transfer area. Therefore, the temperature value at a particular part of the heat exchanger varies where heat is transferred between the hot medium and the heat conducting medium. Logarithmic Mean Temperature Difference is the temperature distribution value that can occur in a heat exchanger.

A better heat transfer value in counter-flow requires a smaller heat transfer surface with the same heat transfer value (Rajput, 2012).

The LMTD value of the temperature distribution in Figure 8 for a counter-flow heat exchanger can be determined using equation 4, where θ_m is 65°C.

The heat exchanger analysis has the most uncertain and important part, namely determining the overall heat transfer coefficient. The coefficient is the total thermal resistance to heat transfer between two fluids (Bergman & Lavine, 2017).

Table 6. Brine Temperature 103,36 °C Heat Transfer Energy

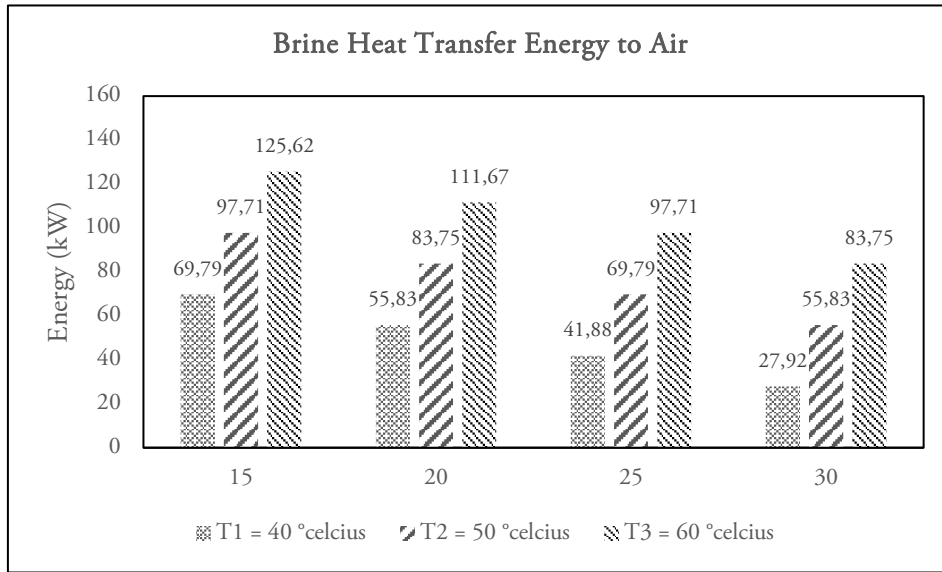| Ambient Air Temperature (°C)	Brine Heat Transfer Energy to Air (kW)		
	T1 = 40 °C	T2 = 50 °C	T3 = 60 °C
15	69,79	97,71	125,62
20	55,83	83,75	111,67
25	41,88	69,79	97,71
30	27,92	55,83	83,75

Figure 7. Energy Graph of Brine to Air Heat Transfer
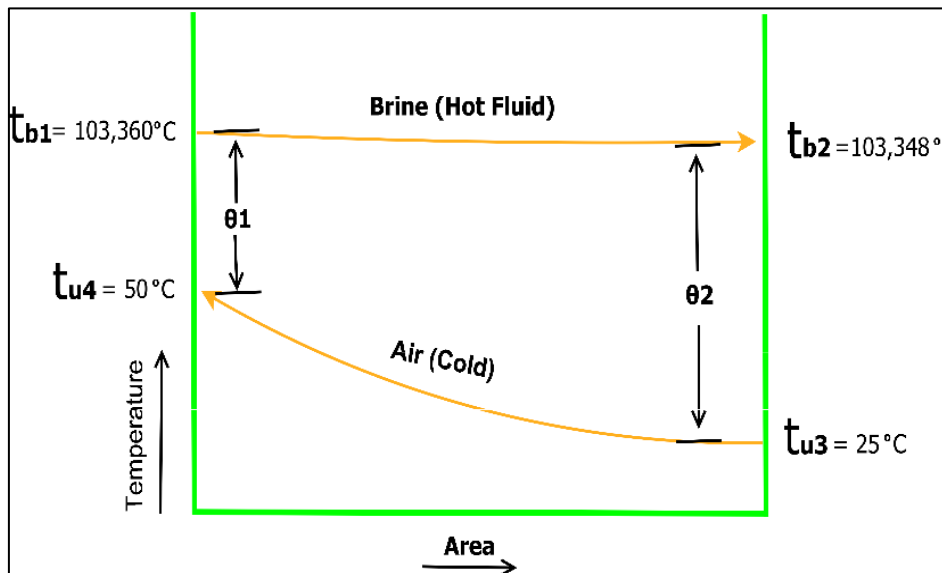
Figure 8. Research Data Collection Point

From equation 5, assuming the overall heat transfer coefficient in the heat exchanger is 1070 W/m².K, the overall heat transfer coefficient of the steam condenser (water in tubes) is 1000-6000 W/m².K (Bergman & Lavine, 2017), then the heat transfer surface area can be determined by equation 6 with a surface area of A = 1 m². This surface area is the basis of the design of the heat exchanger in the coffee dryer.

3.3. Exergy Calculation Results

The exergy value that occurs in the heat exchanger is determined by the type of heat medium and the heat conducting medium through which the heat exchanger passes. According to (Moran et al., 2014), the calculation of exergy in this study can be determined with the following assumptions of the technical modelling:

- There is no significant transfer of heat energy from the system to the environment.
- Changes in kinetic energy and potential energy at the inlet and outlet flows of the heat exchanger are negligible.
- Air is modelled as an ideal gas.
- Environmental temperature and pressure reference based on ambient air conditions

The information in Table 7 can be used to determine the exergy value of heat transfer from brine as a hot medium using equation 7. Regarding the enthalpy of brine output and the enthalpy of brine input, the environmental reference temperature in T_o and the entropy values of the output brine and the input brine, the exergy value of the brine is $m(e_2 - e_1) = -70$ kW. The minus value of exergy indicates that the energy released by brine in the heat exchanger is -70 kW.

From the data in Table 8, it can be determined the exergy value of air as a heat conducting medium using equation 8 regarding the enthalpy value of the output air and the enthalpy of the input air, the environmental

reference temperature in T_o and the entropy value of the output air, the intake air, and the ideal gas value. The exergy value of air is obtained from the air of $m(e_4 - e_3) = 3$ kW. The positive exergy value indicates that the energy received by the air in the heat exchanger to raise the temperature is 3 kW.

From the brine exergy value and the air exergy value, it can be determined how much of the exergy destruction value occurs in the heat exchanger by using equation 9 with the obtained exergy destruction of $E_d = -67$ kW. From the calculation results, the exergy destruction value that occurs in the heat exchanger is -67 kW, which means much energy that is not maximally used in the heat exchanger.

Table 7. Enthalpy and Entropy Values of Brine

Parameter	Brine			
	Value	Units	Source	Information
Mass (m)	1.382,892	Kg/s	Primary data	Brine Input
Enthalpy-1 (hf1)	433,239	kJ/kg	Table A-2 (T1 = 103,360 °C)	Interpolation
Enthalpy-2 (hf2)	433,189	kJ/kg	Table A-2 (T2 = 103,348 °C)	Interpolation
Entropy-1 (sf1)	1,34440	kJ/kg.K	Table A-2 (T1 = 103,360 °C)	Interpolation
Entropy-2 (sf2)	1,34426	kJ/kg.K	Table A-2 (T2 = 103,348 °C)	Interpolation
Ambient temperature (To)	298,15	Kelvin	25 °C	Environmental Reference : Air

Table 8. Enthalpy and Entropy Values of Air

Parameter	Brine			
	Value	Units	Source	Information
Mass (m)	2,78	Kg/s	Primary data	Air Input
Enthalpy-3 (h3)	298,333	kJ/kg	Table A-22 (T3 = 298,15 K)	Interpolation
Enthalpy-4 (h4)	323,4526	kJ/kg	Table A-22 (T4 = 323,15 K)	Interpolation
Entropy-3 (so3)	1,695785	kJ/kg.K	Table A-22 (T3 = 298,15 K)	Interpolation
Entropy-4 (so4)	1,776722	kJ/kg.K	Table A-22 (T4 = 323,15 K)	Interpolation
Ambient temperature (To)	298,15	Kelvin	25 °C	Environmental Reference: Air Constant
Air molecular weight (M)	28,97	Kg/mol	Ideal Gas	
Pressure-3 (P3)	2	Barg		Assumption
Pressure-4 (P4)	2	Barg		Assumption

3.4. DWSIM Simulation Results

The heat exchanger can be simulated using DWSIM software to determine the temperature value and the energy that can be generated from the heat transfer that occurs from both the heat medium and the heat conductor, as shown in Figure 9. Furthermore, the results of this simulation can be compared with the results of manual calculations to find out that there is no significant difference between the simulation results and manual calculations.

Table 9 shows the heat exchanger and brine and air simulation results. The simulation results of a counter-flow heat exchanger for an air temperature of 25 °C increased to 50 °C showed a heat load of 69.6179 kW with an LMTD of 65 °C.
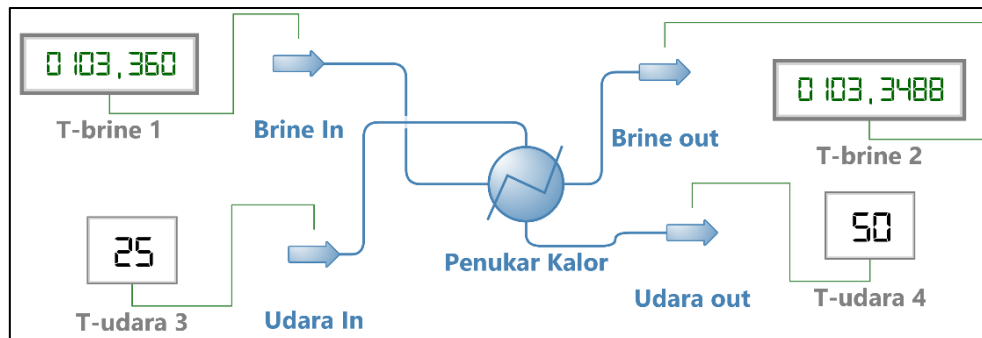

Figure 9. Simulation of a DWSIM Heat Exchanger

Table 9. (A) Heat Exchanger, (B) Brine and Air Simulation Results

Heat Exchanger (A)		
Object	Heat Exchanger	
Global Heat Transfer Coefficient (U)	1070,11	W/[m².K]
Heat Exchanger Area (A)	1	m2
Heat Load	69,6179	kW
Cold Fluid Outlet Temperature	50	C
Hot Fluid Temperature	103,349	C
Logarithmic Mean Temperature Difference LMTD	65,0565	C
Thermal Efficiency	31,8163	%

Brine and Air (B)					
Object	Brine In	Brine Out	Air in	Air out	
Temperature	103,36	103,349	25	50	C
Pressure	6,52	6,52	2	2	Bar
Mass Flow	4,97841E+06	4,97841E+06	10000	10000	Kg/h
Molecular Weight (Vapour)	0	0	28,96	28,96	Kg/mol
Heat Capacity (Liquid 1)	4,22135	4,22134	0	0	Kj/[kg.K]
Phases	Liquid Only	Liquid Only	Vapour Only	Vapour Only	
Ideal Gas Heat Capacity Cp (Vapour)	1,89235	1,01848	1,00142	1,00365	Kj/kg

Table 10. Heat Transfer Energy Temperature 103,36°C Simulation Results

Ambient Air Temperature (°C)	Brine Heat Transfer Energy to Air (kW)		
	T1 = 40 °C	T2 = 50 °C	T3 = 60 °C
15	69,56	97,42	125,32
20	55,66	83,52	111,42
25	41,75	69,62	97,51
30	27,84	55,71	83,60

Table 10 above shows the simulation results of heat transfer energy from brine to air. The resulting energy value is almost the same as the manual calculations using equation 1. Therefore, the standard deviation between manual calculations and simulations is set at a minimum value of 0.056569 and a maximum value of 0.212132.

3.5. Silica Scale Formation Rate

The performance of the heat exchanger depends on the heat transfer between the two media that exchange heat energy. Silica is a substance found in geothermal fluids. Silica can form a scale on the heat exchanger, which causes a decrease in performance due to the thickening of the heat exchanger material, according to research that has been carried out (Sarulla Operation Ltd., 2021) to determine the rate of silica formation from reinjection fluid at the Sarulla power plant. The results showed a decrease in the OEC brine output temperature caused by increased electricity production to maximize the available brine. The OEC brine output temperature is 105°C - 110°C from the initial temperature of 129°C. The results showed that to get a low silica deposition rate of < 1 mm/year, the temperature must be >104°C and pH < 4. The heat exchanger in this study used hot media in the form of heat from brine with a temperature of 103°C, so the rate of silica formation is >1mm/year. The heat exchanger can still be used with the provision of periodic maintenance of the heat exchanger in the event of a decrease in performance of the heat exchanger. The temperature of the inlet brine can also return to high if the two wells in the maintenance phase are returned to the system.

3.6. Coffee Drying Advantages and Disadvantages

Traditional coffee drying (drying in the open field) carried out by farmers generally has weaknesses. Rain and cloudiness are the main obstacles to traditional drying and can only be done during the day (Yani & Fajrin, 2013b). Meanwhile, drying using residual geothermal fluid through a heat exchanger can dry at night and is available 24 hours a day without being disturbed by the weather. However, drying coffee using a heat exchanger is very expensive. Nevertheless, this can be done away with the help of corporate social responsibility.

3.7. Geothermal CO_2 Emissions

Energy sourced from geothermal has the lowest CO_2 emissions compared to other energy sources such as natural gas, fuel oil, and coal. For example, in Figure 10, geothermal energy produces the smallest emissions among other energy sources in generating electricity and heating power plants compared to coal, which produces the highest emissions in generating electricity and heating power plants. Coffee dryers can also use gas fuel from liquefied petroleum gas (Djafar, Piarah, Djafar, & Riadi, 2018) but still produce high CO_2 emissions compared to geothermal energy. So geothermal energy is perfect for the environment because it produces the most negligible CO_2 emissions.
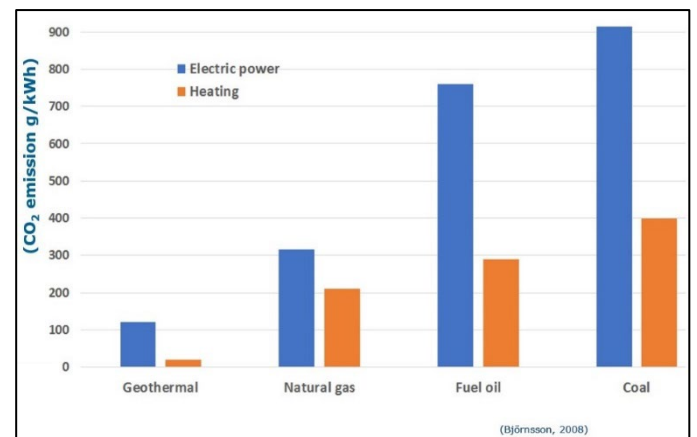

Figure 10. CO_2 Emissions from Electric and Heating Power Plants, From Different Energy Sources (Gissurarson & Arason, 2018)

4. CONCLUSION

Energy from brine reinjection of 70 kW is sufficient to raise the air temperature from 25°C to 50°C with a mass of 10 tons/hour required for drying coffee beans. The exergy destruction value during heat transfer in the heat exchanger at an air temperature of 25°C to 50°C is 67kW. Drying coffee beans does not interfere with the power plant's reinjection system because fluid temperature changes do not change significantly. The rate of silica formation in the reinjection pipe is highly dependent on the temperature and pH of the power plant brine reinjection, so periodic maintenance is required to prevent the heat exchanger from deteriorating. The simulation results have the same results as the manual calculations. The standard deviation between manual calculations and simulations is set at a minimum value of 0.056569 and a maximum value of 0.212132.

REFERENCES

Abdulaziz, A. (2020). Analisis Energi dan Eksergi Terhadap Komponen Utama PLTU Unit 3 Sebelum dan Sesudah Overhaul di PT. Indonesia Power Banten 3 Lontar OMU, 33. Retrieved from http://156.67.221.169/3203/

Ahmad, A. H., Adityatama, D. W., Rusdianto, M. A., Pradana, G. M., Beryll, T. A., Prasetyo, P. V., & Rachmadani, A. (2021). Potential Alternatives for Geothermal Direct Use in Mataloko to Increase Public Acceptance Country United States New Zealand Indonesia, 2025(July), 1–14.

Ariawan, A. M., Windarta, J., & Dwiatmoko, S. (2022). Rooftop PV Plant Development Planning at the Central Java Provincial DPRD Secretariat Office. Jurnal Riset Teknologi Pencegahan Pencemaran Industri, 13.

Australian Academy of Science. (2015). Feeling the heat: geothermal energy. Retrieved from https://www.science.org.au/curious/technology-future/feeling-heat-geothermal-energy

Bergman, T. L., & Lavine, A. S. (2017). Fundamentals of Heat and Mass Transfer (8th ed., Vol. 59).

BMKG. (2022). Stasiun Meteorologi Silangit. Retrieved from https://dataonline.bmkg.go.id/

BPS. (2021). Kabupaten Tapanuli Utara Dalam Angka.

BPTP Lampung. (2018). Teknologi Pascapanen Kopi, Untuk Meningkatkan Mutu Komoditas Unggulan Lampung. Badan Penelitian dan Pengembangan Pertanian Kementerian Pertanian. Retrieved from www.litbang.deptan.go.id

De Sousa, J., & Domenici Roberto, C. (1998). New Technologies for the Drying of Coffee, 1–17.

Djafar, Z., Piarah, W. H., Djafar, Z., & Riadi, R. (2018). Analisis Prestasi Pengering Kopi Berbasis Bahan Bakar Gas (LPG). Prosiding Seminar Ilmiah Nasional Sains Dan Teknologi, 4(November), 399–408.

Fauzi, Z. N., & Widiantoro, H. (2021). Perancangan Mesin Pengering Biji Kopi Semi Otomatis Kapasitas 25 kg.

Finzer, J. R. D., Sfredo, M. A., Sousa, G. D. B., & Limaverde, J. R. (2007). Dispersion coefficient of coffee berries in vibrated bed dryer. Journal of Food Engineering. https://doi.org/10.1016/j.jfoodeng.2006.03.011

Gissurarson, M., & Arason, S. (2018). Geothermal Direct Use. Iceland Geothermal Conference, (April), 75–79.

Gultom, & T., S. S. (2019). Rancang Bangun Dan Pengujian Pengering Biji Kopi Tenaga Listrik Dengan Pemanfaatan Energi Surya. Dinamis. https://doi.org/10.32734/dinamis.v7i4.7201

Hutasoit, P. (2020). Ratusan Massa Demo DPRD Taput, Tuntut PT SOL Tutup, Turunkan Ahli. Retrieved from https://waspada.id/sumut/ratusan-massa-demo-dprd-taput-tuntut-pt-sol-tutup-turunkan-ahli/

IESR. (2021). Indonesia Energy Transition Outlook 2021. Iesr, 1–93.

Kreith, F., Manglik, R. M., & Bohn, M. S. (2011). Principles of Heat Transfer (7th ed.).

Moran, M. J., Shapiro, H. N., Boettner, D. D., & Bailey, M. B. (2014). Fundamentals of Engineering

Thermodynamics. https://doi.org/10.7227/ijmee.29.1.2

Mudassir, R. (2021). Punya Potensi Besar, Energi Panas Bumi Masih Kurang Dimanfaatkan di Indonesia. Retrieved from https://ekonomi.bisnis.com/read/20210926/44/1446892/punya-potensi-besar-energi-panas-bumi-masih-kurang-dimanfaatkan-di-indonesia

Nagel, A., Dwiatmoko, S., & Windarta, J. (2022). Soaking Up The Sun: Designing Small Scale Photovoltaic (PV) Rooftop for Micro, Small, and Medium Enterprises (MSME): Study Case at Rattan Crafts Center in Trangsan Village, Sukoharjo, Central Java. Jurnal Riset Teknologi Pencegahan Pencemaran Industri, 13.

Rajput, E. R. K. (2012). Heat and Mass Transfer. India.

Rakhmadi, R., & Sutiyono, G. (2015). Using Private Finance to Accelerate Geothermal Deployment: Sarulla Geothermal Power Plant, Indonesia.

Rame, R., Purwanto, P., & Sudarno, S. (2021). Environmental Critical Aspects of The Conversion of Biomass to Biogas for Sustainable Energy in Indonesia. Jurnal Riset Teknologi Pencegahan Pencemaran Industri, 12.

Sarulla Operation Ltd. (2021). Pilot Test Low Temperature OEC Brine.

Weather Spark. (2022). Iklim dan Cuaca Rata-rata Sepanjang Tahun di Siborong-Borong. Retrieved from https://id.weatherspark.com/y/112714/Cuaca-Rata-rata-pada-bulan-in-Siborong-Borong-Indonesia-Sepanjang-Tahun

Wolf, N. (2015). Sarulla 330 MW geothermal project key success factors in development. Transactions - Geothermal Resources Council, 39, 907–912.

Yani, E., & Fajrin, S. (2013a). Karakteristik Pengeringan Biji Kopi Berdasarkan Variasi Kecepatan Aliran Udara Pada Solar Dryer.

Yani, E., & Fajrin, S. (2013b). Karakteristik Pengeringan Biji Kopi Berdasarkan Variasi Kecepatan Aliran Udara Pada Solar Dryer. Jurnal Teknika, 20(1), 17–22. Retrieved from https://docplayer.info/31509139-Karakteristik-pengeringan-biji-kopi-berdasarkan-variasi-kecepatan-aliran-udara-pada-solar-dryer.html